Theoretical Investigation on Base-Induced 1,2-Eliminations in the Model System $F^- + CH_3CH_2F$. The Role of the Base as a Catalyst

F. Matthias Bickelhaupt,† Evert Jan Baerends,*,‡ Nico M. M. Nibbering,† and Tom Ziegler§

Contribution from the Instituut voor Massaspectrometrie, Universiteit van Amsterdam, Nieuwe Achtergracht 129, 1018 WS Amsterdam, The Netherlands, Sectie Theoretiche Chemie, Scheikundig Laboratorium, Vrije Universiteit, De Boelelaan 1083, 1081 HV Amsterdam, The Netherlands, and Department of Chemistry, University of Calgary, Calgary, Alberta, Canada T2N 1N4

Received March 1, 1993®

Abstract: A theoretical investigation has been performed on the gas-phase reactions of the $F^- + C_2H_5F$ model system using a high-level density-functional method. The purpose is a better understanding of the nature of the base-induced elimination reactions, in particular the role of the base as a catalyst, the prevalence of anti-E2 over syn-E2 elimination, the prevalence of E2 elimination over S_N2 substitution, and the reaction mechanism. The base has been found to play a key role as a catalyst. The uncatalyzed transition-state (TS) energies are very high. The uncatalyzed syn TS is lowest, in contrast to the prevalent view that the anti TS would be more strongly stabilized by favorable interaction of the developing carbanionic lone pair at C^β with the backside lobe of the $\sigma^*(C^\alpha–F)$. Upon catalysis by the base, the transition state of the anti mode is selectively stabilized, leading to the prevalence of anti-E2 over syn-E2 elimination. One reason for the selective stabilization is the favorable electrostatic interaction of the F^- base with the C^α–F dipole of the anti TS. A second factor is the very low energy and, thus, the good acceptor capability of the C_2H_5F 8a′ LUMO in the strongly rearranging, loose anti-E2 transition state. The anti-E2 elimination prevails over the S_N2 substitution. This is ascribed to the lower energy and entropy barrier for the anti-E2 elimination as well as to the preferential formation of a reactant complex which is predestined to react further via the anti-E2 pathway. The anti-E2 elimination (and not only the syn-E2) is found to preferentially produce FHF^- and C_2H_4. The prevalence of anti-E2 over S_N2 is therefore in excellent agreement with the experimental result that reaction of F^- and C_2H_5F exclusively yields FHF^- and C_2H_4. However, we reinterpret this observation as being the result of anti-E2 and not syn-E2 elimination. A qualitative MO theoretical analysis is given, which enables one to understand the coplanarity of the reaction and to predict which reaction, E2 or S_N2, dominates for a given general substrate C_2H_5L (Scheme III). On the basis of a simple MO theoretical concept, an "E2/S_N2 spectrum" is proposed, which comprises the Bunnet–Cram E2H and the Winstein–Parker E2H/E2C as well as the S_N2/S_N1 mechanistic spectra. The base-induced eliminations studied are of the E2H category. No E2C-like interactions are present in the transition state. An intermediate anion is never formed. The syn-E2 reaction is only slightly E1cb-like, whereas the anti-E2 elimination is virtually ideal E2. Intrestingly, there is no distinct channel on the anti-E2 reaction energy surface leading from the reactant complex to the transition state. Instead, the system shows a very weak tendency to proceed via an E1cb-like route (initial C^β–H bond elongation) or via an E1-like route (initial C^α–F bond elongation). An important characteristic of the anti-E2 elimination, which is not contained in the E2H formalism, is the pronounced shift of the abstracted proton from the C^β to the C^α position in the transition state.

1. Introduction

Base-induced 1,2-elimination reactions (E2: eq 1a) constitute one of the basic types of reactions in organic chemistry.[1,2] They are an important tool to introduce double bonds between carbons and/or heteroatoms in organic synthesis.[1-6] An alternative reaction pathway for a base and a substrate containing a leaving group is nucleophilic substitution (S_N2: eq 1b). Therefore, E2

$$B^- + H\text{-}C^\beta H_2\text{-}C^\alpha H_2\text{-}L \xrightarrow{E2} B\text{-}H + CH_2{=}CH_2 + L^- \quad (1a)$$

$$B^- + H\text{-}C^\beta H_2\text{-}C^\alpha H_2\text{-}L \xrightarrow{S_N2} CH_3\text{-}CH_2\text{-}B + L^- \quad (1b)$$

and S_N2 reactions can be in competition and may occur as unwanted side reactions of each other.[1,2]

Extensive experimental investigations on base-induced elimination reactions have been performed in the condensed phase[7-18]

† Universiteit van Amsterdam.
‡ Vrije Universiteit.
§ University of Calgary.
® Abstract published in *Advance ACS Abstracts*, September 1, 1993.

(1) Carey, F. A.; Sundberg, R. J. *Advanced Organic Chemistry*; Plenum Press: New York, 1984; Part A.
(2) Lowry, T. H.; Richardson, K. S. *Mechanism and Theory in Organic Chemistry*, 2nd ed.; Harper and Row: New York, 1981.
(3) Cockerill, A. F.; Harrison, R. G. In *The Chemistry of Double Bonded Functional Groups*; Patai, S., Ed.; Wiley: London, 1977; Supplement A, Part 1, Chapter 4.
(4) Kice, J. L.; Kopczyk-Subotkowska, L. *J. Org. Chem.* **1990**, *55*, 1523 and references cited therein.
(5) Cullis, C. F.; Fish, A. In *The Chemistry of the Carbonyl Group*; Patai, S., Ed.; Wiley: London, 1966; pp 142–143.
(6) *Multiple Bonds and Low Coordination in Phosphorus Chemistry*; Regitz, M., Scherer, O. J., Eds.; Georg Thieme Verlag: Stuttgart, Germany, 1990; in particular Chapter D.4 (Appel, R.), Chapter D.8 (Niecke, E.), and Chapter D.9 (Yoshifuji, M.).
(7) Gandler, J. R. In *The Chemistry of Double-Bonded Functional Groups*; Patai, S., Ed.; Wiley: New York, 1989; Vol. 2, Part I.
(8) Bartsch, R. A.; Závada, J. *Chem. Rev.* **1980**, *80*, 453.
(9) Saunders, W. H., Jr. *Acc. Chem. Res.* **1976**, *9*, 19.
(10) Bartsch, R. A. *Acc. Chem. Res.* **1975**, *8*, 239.
(11) Saunders, W. H., Jr.; Cockerill, A. F. *Mechanisms of Elimination Reactions*; Wiley: New York, 1973; Chapter 1.
(12) Cram, D. J.; Greene, F. D.; DePuy, C. H. *J. Am. Chem. Soc.* **1956**, *78*, 790.
(13) Bunnett, J. F. *Angew. Chem.* **1962**, *74*, 731.

0002-7863/93/1515-9160$04.00/0

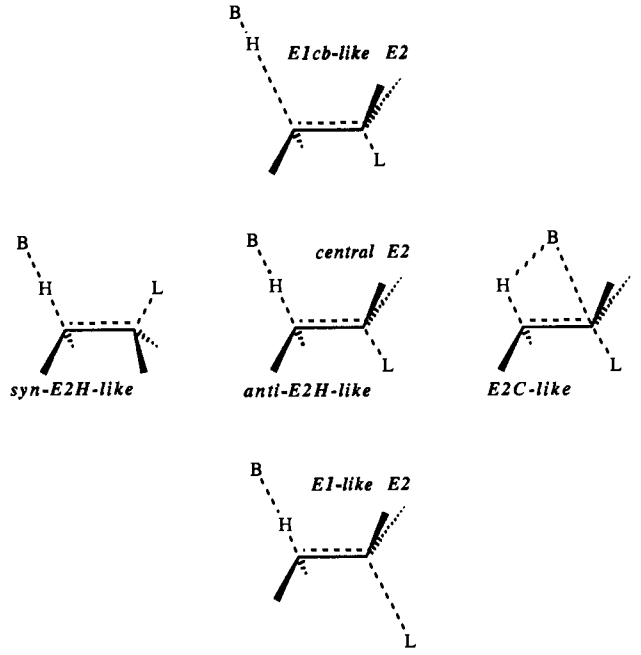

Figure 1. Mechanistic spectrum of transition states in base-induced 1,2-elimination reactions.

as well as in the gas phase.[19-33] Considerable experience has been gathered concerning the parameters that determine the reaction rates, the product distribution, and the stereochemistry, i.e. syn- or anti- (coplanar) E2 elimination (Figure 1). An important concept in the description and classification of elimination reactions is the variable transition state (VTS).[1,2] In the VTS theory, the reactions are classified according to the geometry of the transition state (TS), which is conceived to be located at one point in a continuous spectrum of mechanistic possibilities. The VTS theory comprises the Bunnett–Cram E2H spectrum,[12-14] i.e. E1cb (-like), synchronous E2, and E1 (-like) eliminations involving linear proton transfer, as well as the Winstein–Parker E2H/E2C spectrum[15,16] in which bent proton transfer may occur with a certain degree of base/C^α covalent interaction (Figure 1).

Gas-phase experiments[19-33] enabled the study of the intrinsic reactivity of reaction systems without the effect of solvent molecules and counter ions.[32,33] An important feature which distinguishes gas-phase from condensed-phase reactions is the prominent role that ion/molecule complexes play.[32-34] The double-well potential, first suggested for gas-phase S_N2 reactions on the basis of experiments by Olmstead and Brauman,[35] has been confirmed by *ab initio* calculations[36-45] and is now generally accepted for gas-phase reactions.[32,33] Very recently, the intermediate reactant and product complexes of gas-phase ion/molecule S_N2 reactions were isolated and studied experimentally.[46-48]

Base-induced E2 elimination reactions have received relatively little attention in theoretical studies[38,49-63] if compared to S_N2 substitutions (see, for instance, refs 36–45). This may be due to the more extensive and complex reorganization of bond making and bond breaking during the E2 reaction which complicates the finding of the transition state. Early semiempirical calculations of Fukui et al.[49,50] have shown that the coplanar stereochemistry of E2 reactions can be ascribed to the frontier MO electronic coupling between the leaving group and the H^β which has to be abstracted. This is revealed by a higher amplitude on H^β and a stronger C^β–H antibonding character of the substrate LUMO, which accepts charge from the HOMO of the attacking base, if the H^β and the leaving group are anti or syn coplanar. The interdependence of the C^β–H and the C^α–F bonds via delocalized MOs in E2 reactions has been pointed out by others[51-58] and has been related to the mechanism of spin coupling in NMR.[53] In the prevalent view that a carbanionic lone pair at C^β develops while the H^β is abstracted by the base,[54] the preference for anti over syn elimination could be ascribed to stabilization of the anti TS by favorable interaction of this lone pair with the backside lobe of the $\sigma^*(C^\alpha$–F) orbital. It would thus be related to the phenomena of the anomeric effect and the effect of anionic hyperconjugation on rotational barriers[64,65] (see also ref 72, Chapter 10). Furthermore, important quantities related to the E2 reaction such as reaction and activation energies as well as transition-state structures have been determined.[55,56]

(14) Bartsch, R. A.; Bunnett, J. F. *J. Am. Chem. Soc.* **1968**, *90*, 408.
(15) Parker, A. J.; Ruane, M.; Biale, G.; Winstein, S. *Tetrahedron Lett.* **1968**, 2113.
(16) Biale, G.; Cook, D.; Lloyd, D. J.; Parker, A. J.; Stevens, I. D. R.; Takahashi, J.; Winstein, S. *J. Am. Chem. Soc.* **1971**, *93*, 4735.
(17) McLennan, D. J. *Tetrahedron* **1975**, *31*, 2999.
(18) Hoffman, R. V.; Bartsch, R. A.; Cho, B. R. *Acc. Chem. Res.* **1989**, *22*, 211 and references cited therein.
(19) de Koning, L. J.; Nibbering, N. M. M. *J. Am. Chem. Soc.* **1987**, *109*, 1715.
(20) van Berkel, W. W.; de Koning, L. J.; Nibbering, N. M. M. *J. Am. Chem. Soc.* **1987**, *109*, 7602.
(21) de Koning, L. J.; Nibbering, N. M. M. *J. Am. Chem. Soc.* **1988**, *110*, 2066.
(22) Ridge, D. P.; Beauchamp, J. L. *J. Am. Chem. Soc.* **1974**, *96*, 637.
(23) Ridge, D. P.; Beauchamp, J. L. *J. Am. Chem. Soc.* **1974**, *96*, 3595.
(24) Sullivan, S. A.; Beauchamp, J. L. *J. Am. Chem. Soc.* **1976**, *98*, 1160.
(25) van Doorn, R.; Jennings, K. R. *Org. Mass Spectrom.* **1981**, *16*, 397.
(26) DePuy, C. H.; Bierbaum, V. M. *J. Am. Chem. Soc.* **1981**, *103*, 5034.
(27) DePuy, C. H.; Beedle, E. C.; Bierbaum, V. M. *J. Am. Chem. Soc.* **1982**, *104*, 6483.
(28) Bierbaum, V. M.; Filley, J.; DePuy, C. H.; Jarrold, M. F.; Bowers, M. T. *J. Am. Chem. Soc.* **1985**, *107*, 2818.
(29) Thomas, D. A.; Bloor, J. E.; Bartmess, J. E. *J. Am. Soc. Mass Spectrom.* **1990**, *1*, 295.
(30) Grabowski, J. J.; Zhang, L. *J. Am. Chem. Soc.* **1989**, *111*, 1193.
(31) Noest, A. J.; Nibbering, N. M. M. *Adv. Mass Spectrom.* **1980**, *8A*, 227.
(32) Nibbering, N. M. M. *Acc. Chem. Res.* **1990**, *23*, 279.
(33) Nibbering, N. M. M. *Adv. Phys. Org. Chem.* **1988**, *24*, 1.
(34) Lias, S. G.; Ausloos, P. *Ion-Molecule Reactions*; American Chemical Society: Washington, DC, 1975.
(35) Olmstead, W. N.; Brauman, J. I. *J. Am. Chem. Soc.* **1977**, *99*, 4219.
(36) Sini, G.; Shaik, S.; Hiberty, P. C. *J. Chem. Soc., Perkin Trans. 2* **1992**, 1019.
(37) Shi, Z.; Boyd, R. J. *J. Am. Chem. Soc.* **1991**, *113*, 1072.
(38) Zahradník, R.; Hess, B. A., Jr. *J. Mol. Struct. (THEOCHEM)* **1991**, *230*, 387.
(39) Zhao, X. G.; Tucker, S. C.; Truhlar, D. G. *J. Am. Chem. Soc.* **1991**, *113*, 826.
(40) Tucker, S. C.; Truhlar, D. G. *J. Am. Chem. Soc.* **1990**, *112*, 3338.
(41) Vande Linde, S. R.; Hase, W. L. *J. Phys. Chem.* **1990**, *94*, 6148.
(42) Ohta, K.; Morokuma, K. *J. Phys. Chem.* **1985**, *89*, 5845.
(43) Morokuma, K. *J. Am. Chem. Soc.* **1982**, *104*, 3732.
(44) Wolfe, S.; Mitchell, D. J.; Schlegel, H. B. *J. Am. Chem. Soc.* **1981**, *103*, 7692, 7694.
(45) Dedieu, A.; Veillard, A. *J. Am. Chem. Soc.* **1972**, *94*, 6730.
(46) Graul, S. T.; Bowers, M. T. *J. Am. Chem. Soc.* **1991**, *113*, 9696.
(47) Cyr, D. M.; Posey, L. A.; Bishea, G. A.; Han, C.-C.; Johnson, M. A. *J. Am. Chem. Soc.* **1991**, *113*, 9697.
(48) Wilbur, J. L.; Brauman, J. I. *J. Am. Chem. Soc.* **1991**, *113*, 9699.
(49) Fukui, K.; Hao, H.; Fujimoto, H. *Bull. Chem. Soc. Jpn.* **1969**, *42*, 348.
(50) Fujimoto, H.; Yamabe, S.; Fukui, K. *Bull. Chem. Soc. Jpn.* **1971**, *44*, 971.
(51) Ito, S.; Kakehi, A. *Bull. Chem. Soc. Jpn.* **1990**, *63*, 2850.
(52) Hudson, R. F. *J. Mol. Struct. (THEOCHEM)* **1992**, *261*, 91.
(53) Lowe, J. P. *J. Am. Chem. Soc.* **1972**, *94*, 3718.
(54) Bach, R. D.; Badger, R. C.; Lang, T. J. *J. Am. Chem. Soc.* **1979**, *101*, 2845.
(55) Minato, T.; Yamabe, S. *J. Am. Chem. Soc.* **1985**, *107*, 4621.
(56) Minato, T.; Yambe, S. *J. Am. Chem. Soc.* **1988**, *110*, 4586.
(57) Nguyen, M. T.; Clarke, L. F.; Hegarty, A. F. *J. Org. Chem.* **1990**, *55*, 6177.
(58) Lee, I.; Park, H. Y.; Lee, B.-S.; Kong, B. H.; Lee, B. C. *J. Phys. Org. Chem.* **1992**, *5*, 259.
(59) Pross, A.; Shaik, S. S. *J. Am. Chem. Soc.* **1982**, *104*, 187.
(60) Gronert, S. *J. Am. Chem. Soc.* **1991**, *113*, 6041.
(61) Gronert, S. *J. Am. Chem. Soc.* **1992**, *114*, 2349.
(62) Dewar, M. J. S.; Yuan, Y.-C. *J. Am. Chem. Soc.* **1990**, *112*, 2088.
(63) Dewar, M. J. S.; Yuan, Y.-C. *J. Am. Chem. Soc.* **1990**, *112*, 2095.
(64) Hoffmann, R.; Radom, L.; Pople, J. A.; Schleyer, P. v. R.; Hehre, W. J.; Salem, L. *J. Am. Chem. Soc.* **1972**, *94*, 6221.
(65) Schleyer, P. v. R.; Kos, A. J. *Tetrahedron* **1983**, *39*, 1141.

Still, however, a number of interesting questions remain which are not completely understood. Of particular interest is the question of the magnitude and the mechanism of the catalytic effect of the base in the E2 reaction. How much does the base lower the transtion-state energies, would the uncatalyzed anti-E2 elimination already prevail over syn-E2, as expected from the above qualitative MO argument, or is actually the TS of the syn-E2 elimination more stable than that of the anti-E2 elimination because of a favorable interaction between the leaving group L^- and the β-proton which is abstracted? Is the catalysis of the attacking base selective in the sense that it is decisive in determining the prevalence of anti over syn elimination?

The purpose of the present paper is to answer these and other questions, in order to arrive at a better understanding of the nature of base-induced E2 reactions. To this end, a theoretical investigation on the anti- and syn-E2 reactions of the fluoride/fluoroethane (B^-, $L^- = F^-$ in eq 1) model reaction system has been carried out. The S_N2 substitution of F^- on C_2H_5F has been included in our study for completeness and for a better comparison with previous theoretical[55,56] and experimental (ICR) gas-phase[22-24] investigations on this reaction system.

In the context of the VTS concept (*vide supra*), it is interesting to know the location of reactant and product complexes as well as transition states on the two-dimensional reaction energy surface $E(d(C^\beta\text{–H}), d(C^\alpha\text{–F}))$ of the E2 reaction. Moreover, the shape of this reaction energy surface contains important information on the way that the reaction system can proceed from the reactant configuration to the product configuration, i.e., information on the character of the reaction. Therefore, in the present theoretical study, not only stationary points but the complete two-dimensional reaction energy surface, $E(d(C^\beta\text{–H}), d(C^\alpha\text{–F}))$, has been determined for the anti-E2 and syn-E2 reactions. Structures and relative energies for the relevant stationary points of the E2 and S_N2 reaction systems have been obtained. The quantitative results, including an estimate of the catalytic effect of the base on the 1,2-elimination, are discussed and explained on the basis of a detailed analysis of the electronic structure of and bonding between the reactants in E2 reactant complexes and transition states. Furthermore, a qualitative MO theoretical analysis is given which enables one to understand and predict which reaction, E2 or S_N2, dominates for a given general substrate C_2H_5L. From this analysis a simple MO theoretical concept evolves which enables one to connect the VTS model for E2 and S_N2 reactions, resulting in an "E2/S_N2 spectrum" of reaction mechanisms.

The calculations were performed using a high-level density-functional (DF) method[66,67] as implemented in the Amsterdam density-functional (ADF) program system.[68-71] Since the one-electron picture is preserved in the Kohn–Sham approach to density-functional theory (DFT),[67] the interpretation of the bonding can be cast in familiar terms such as exchange or Pauli repulsion and donor/acceptor interactions.[72]

2. Method

General Procedure. The MOs were expanded in two different uncontracted sets of Slater-type orbitals (STOs), i.e. the DZP and the TZPP basis sets. The DZP basis, used in the geometry optimization, is of double-ζ quality (two STOs per *nl* shell), with a polarization function added on each atom: 3d on C and F, 2p on H. The TZPP basis, used in single point energy calculations, is of triple-ζ quality and has been augmented with two polarization functions on each atom (3d and 4f on C and F, 2p and 3d on H). It has been noticed before that the complexation energy of fluorine-containing anion/molecule complexes, which depends very critically on the quality of the basis set, can be described satisfactorily with this basis set.[73] The $1s^2$ configuration was assigned to the carbon and fluorine core and was treated by the frozen-core approximation[68] using five 1s STOs in both the DZP and TZPP basis sets. An alternative description of our STO basis sets would be 5-11S** and 5-111S(3d4f,2p3d), using the notation of conventional *ab initio* methods. These STO basis sets should be superior to 6-33G** and 6-333G(3d4f,2p3d) GTO-type basis sets, respectively.

Geometries were optimized with the simple Xα exchange-correlation potential[66] using gradient techniques[74] for minimum energy structures and for the S_N2 transition state, and a procedure described below for anti- and syn-E2 transition states (Xα/DZP level of theory, Figure 2). All stationary points were subjected to a vibrational analysis.

All data in Table I correspond to equilibrium and transition-state structures optimized at the Xα/DZP level of theory. Energies were evaluated by the Xα and LDA/NL methods (local density approximation with nonlocal corrections) by employing the DZP and TZPP basis sets. At the LDA/NL level, exchange is described with Slater's $\rho^{1/3}$ potential (Xα and $\alpha = {}^2/_3$), with a nonlocal correction due to Becke.[75-77] According to the suggestion by Stoll et al.,[78] only correlation between electrons of different spin is introduced, for which electron gas data (in the Vosko–Wilk–Nusair[79] parametrization) are used.

Considerable experience shows that with the DF approach interaction energies in systems involving main group elements

Table I. Calculated Energies, ΔE (eV) (1 eV = 23.06 kcal/mol), of anti-E2, syn-E2, and S_N2 Reaction Systems Relative to the Energy of the Separated Reactants F^- and Staggered CH_3CH_2F (R(st))[a]

system		ΔE		
		Xα/DZP[b]	LDA/NL/DZP[b]	LDA/NL/TZPP[b]
	Reactants			
R(st)	(F^- + st-C_2H_5F)	0.00	0.00	0.00
R(ecl)	(F^- + ecl-C_2H_5F)	0.08	0.07	0.10
	Reactant Complexes			
RC(st)	([F^-, st-C_2H_5F])	−1.91	−1.18	−0.46
RC(ecl)	([F^-, ecl-C_2H_5F])	−1.63	−0.87	−0.11
RC(α)	([F^-, st-C_2H_5F]$_\alpha$)	−1.61	−1.03	−0.43
	Transition States			
TS	(anti-E2)	−0.89	−0.85	−0.41
TS	(syn-E2)	−1.29	−0.75	−0.02
TS	(S_N2)	−1.06	−0.53	−0.02
UTS(anti-E)[c] + F^-		6.20	5.51	5.48
UTS(syn-E)[c] + F^-		3.74	3.53	3.60
	Product Complexes			
PC1	([FHF^-, C_2H_4]$_\pi$)	−2.31	−2.07	−1.36
PC2	([FHF^-, C_2H_4]$_H$)	−2.66	−2.51	−1.78
PC3	([HF, C_2H_4, F^-])	−1.40	−1.08	−0.37
	Products			
P1	(FHF^- + C_2H_4)	−2.05	−2.25	−1.75
P2	(HF + [C_2H_4, F^-])	−0.45	−0.58	0.02
P3	(HF + C_2H_4 + F^-)	1.22	0.41	0.29

[a] See Figure 2 for structures and Figure 3 for graphical representation of LDA/NL/TZPP[b] results. [b] Level of theory: "density-functional"/"basis set". The geometries are obtained at the Xα/DZP level (see the Method). [c] Uncatalyzed transition state (UTS): C_2H_5F fragment (separate from and non-interacting with F^- base), deformed to its geometry in the corresponding transition state; i.e. "UTS = TS − F^-".

(66) Slater, J. C. *Quantum Theory of Molecules and Solids*; McGraw-Hill: New York, 1974; Vol. 4.
(67) Parr, R. G.; Yang, W. *Density-Functional Theory of Atoms and Molecules*; Oxford University Press: New York, 1989.
(68) Baerends, E. J.; Ellis, D. E.; Ros, P. *Chem. Phys.* **1973**, *2*, 41.
(69) Boerrigter, P. M.; Velde, G. te; Baerends, E. J. *Int. J. Quantum Chem.* **1988**, *33*, 87.
(70) Baerends, E. J.; Ros, P. *Chem. Phys.* **1975**, *8*, 412.
(71) Baerends, E. J.; Ros, P. *Int. J. Quantum Chem., Quantum Chem. Symp.* **1978**, *S12*, 169.
(72) Albright, T. A.; Burdett, J. K.; Whangbo, M.-H. *Orbital Interactions in Chemistry*; Wiley: New York, 1985.
(73) Bickelhaupt, F. M.; de Koning, L. J.; Nibbering, N. M. M.; Baerends, E. J. *J. Phys. Org. Chem.* **1992**, *5*, 179.
(74) Versluis, L.; Ziegler, T. *J. Chem. Phys.* **1988**, *88*, 322.
(75) Becke, A. D. *Int. J. Quantum Chem.* **1983**, *23*, 1915.
(76) Becke, A. D. *J. Chem. Phys.* **1986**, *85*, 7184.
(77) Ziegler, T.; Tschinke, V.; Becke, A. *Polyhedron* **1987**, *6*, 685.
(78) Stoll, H.; Golka, E.; Preus, H. *Theor. Chim. Acta* **1980**, *55*, 29.
(79) Vosko, S. H.; Wilk, L.; Nusair, M. *Can. J. Phys.* **1980**, *58*, 1200.

and/or metals, including anion/molecule complexes, in general can be calculated with an accuracy in the order of a few tenths of an electronvolt (ca. 5 kcal/mol) (1 eV = 23.06 kcal/mol).[73,74,80-86]

An analysis of the bonding mechanism[80,87] in F^-/C_2H_5F anti- and syn-E2 reactant complexes and transition states has been performed at the LDA/NL/DZP level (Table II). In this analysis, the interaction energy, $\Delta E_{int} = \Delta E^\circ + \Delta E_{oi}$, is explicitly split up in the steric repulsion ΔE° and the orbital interaction ΔE_{oi}. The steric repulsion, $\Delta E^\circ = \Delta E_{elstat} + \Delta E_{Pauli}$, comprises both the classical electrostatic interaction (ΔE_{elstat}) between the unperturbed charge distributions of the fragments and the four-electron destabilizing interactions between occupied orbitals (Pauli repulsion: ΔE_{Pauli}). The orbital interaction, ΔE_{oi}, accounts for charge transfer (interaction between occupied orbitals on one moiety with unoccupied orbitals of the other, including the HOMO–LUMO interactions) and polarization (empty/occupied orbital mixing on one fragment).

Two-Dimensional Reaction Energy Surfaces and Transition States. The saddle points on the reaction energy surface, $E(d(C^\beta\text{–}H), d(C^\alpha\text{–}F))$, for the syn-E2 and especially for the anti-E2 reaction of F^- and C_2H_5F appear to be located on extremely shallow saddle regions (Figure 4). This easily leads to an erroneous determination of the position of these saddle points. This problem has been circumvented by the determination of the complete reaction energy surfaces $E(d(C^\beta\text{–}H), d(C^\alpha\text{–}F))$. This allows for a more correct determination of TS structures and, further, leads to a better insight into the nature of the reaction. Starting from the reactant complexes, the reaction energy surfaces are determined by stepwise elongation of $d(C^\beta\text{–}H)$ and $d(C^\alpha\text{–}F)$. After each step the geometry is allowed to relax; however, the length of $d(C^\beta\text{–}H)$ and $d(C^\alpha\text{–}F)$ is kept fixed and C_s point group symmetry is superimposed. As a result, one acquires a set of energies in a grid of ($d(C^\beta\text{–}H)$, $d(C^\alpha\text{–}F)$) points on the two-dimensional reaction energy surface (anti-E2 surface, 89 points; syn-E2 surface, 39 points). The reaction energy surfaces are visualized as the contour plots of fifth-order polynomials, which have been fitted to the set of points (Figure 4).

The saddle-point structures determined in this way for the two-dimensional (2D) reaction energy surface have been subjected to a vibrational analysis. From this it appears that each 2D-saddle point only has one associated imaginary frequency (Figure 2). Therefore, it corresponds to a first-order saddle point in the complete hyperdimensional energy surface and, thus, represents a proper TS structure.

3. Results

The results of the DF calculations are displayed in Tables I and II, in Figures 2–8, and in Schemes I–III. Table I (energetics) and Figure 2 (structures) summarize the data on the E2 and S_N2 reactions. From Table I it appears that interaction energies decrease when going from the Xα to the LDA/NL level of density-functional theory. This is mainly due to the increasing exchange or Pauli repulsion due to the introduction of nonlocal corrections for the exchange. The interaction energies further decrease when the basis set increases from DZP to TZPP quality. This is ascribed to a selective stabilization of free F^- ions. The fluoride anions "gain" the most from the introduction of more diffuse basis functions if compared to interacting systems where the charge can be delocalized over the entire F^-/C_2H_5F aggregation.

In the thermal elimination of HF from fluoroethane, the uncatalyzed transition state (UTS) for syn elimination is considerably lower in energy than that for anti elimination (Table I). However, upon catalysis by the F^- base, the transition state of the anti elimination is stabilized much (ca. 2 eV) more than that of the syn elimination. This feature is reproduced at all three levels of theory, i.e. Xα/DZP, LDA/NL/DZP, and LDA/NL/TZPP (Table I). An important difference when going from Xα to the more advanced LDA/NL calculations is the crossing of the energy of the TS(anti-E2) and TS(syn-E2), the latter being higher in energy at the LDA/NL level. Apparently, the use of nonlocal corrections to the exchange is essential in the description of the relative energy of the anti-E2 and syn-E2 transition states. The qualitative features of the LDA/NL/DZP and LDA/NL/TZPP calculations are essentially the same.

Structures (Figure 2) and anti- and syn-E2 reaction energy surfaces (Figure 4) have been obtained at the Xα/DZP level. The discussion on the energetics of the E2 and S_N2 reactions is based on the LDA/NL/TZPP results (Figures 3 and 5), whereas the analysis of the electronic structure and the interaction between the reactants in the reactant complexes and transition states is performed at the LDA/NL/DZP level (Table II and Figures 6–8).

The C_2H_5F and F^-/C_2H_5F species have closed shells; the valence electron configurations are $(a')^{14}(a'')^6$ and $(a')^{20}(a'')^8$, respectively. The orbital interactions between the base F^- and the substrate C_2H_5F predominantly, i.e., for more than 90%, occur in the A' symmetry. The results of a detailed analysis of the electronic structure of the substrate are presented in Schemes I–III.

4. Discussion

In the following two subsections, the competition between base-induced E2 and S_N2 reactions and between anti- and syn-E2 elimination is discussed in terms of the energetics and structures of the reaction systems and in terms of the shape of the E2 reaction energy surfaces. After this, the electronic structure of the C_2H_5F substrate is inspected, and the question is addressed as to why the base catalyzes more effectively the anti-E2 than the syn-E2 elimination. Furthermore, a qualitative MO theoretical analysis is given, which enables one to understand and predict which reaction, E2 or S_N2, dominates for a given substrate C_2H_5L. Next, the significance of our results is considered in the context of the variable transition-state (VTS) concept, i.e. the Bunnet–Cram E2H and the Winstein–Parker E2H/E2C mechanistic spectra. Finally, our results are compared with previous theoretical and experimental gas-phase studies, and it is discussed what differences can be expected when going to the condensed phase.

Anti-E2 *versus* S_N2. We first consider the competition between the base-induced anti elimination (anti-E2) and the nucleophilic substitution (S_N2) of F^- and fluoroethane (eq 1; B^-, $L^- = F^-$). Table I shows the energies of the E2 and S_N2 reaction systems relative to the separated reactants F^- and staggered fluoroethane (F^- + st-C_2H_5F, R(st)). The reactants can combine to form a reactant complex (RC) in which the F^- is hydrogen bonded to st-C_2H_5F either via a β- or via an α-hydrogen: RC(st) and RC(α), respectively (Figure 2). The most stable reactant complex is RC(st) with a complexation energy, $\Delta E_{complex}$, of –0.46 eV, to be compared with –0.43 eV for RC(α) (Table I). In RC(st), the C^β–H bond (1.394 Å) and C^α–F bond (1.503 Å) have already been elongated considerably by 25% and 7%, respectively, while the C–C bond (1.417 Å) has been contracted by 5% with respect to the reactant st-C_2H_5F (Figure 2). The structural change of the st-C_2H_5F fragment in RC(st) can be understood on the basis of the donor/acceptor interaction between the base HOMO, i.e.

(80) Bickelhaupt, F. M.; Nibbering, N. M. M.; van Wezenbeek, E. M.; Baerends, E. J. *J. Phys. Chem.* **1992**, *96*, 4864 and references cited therein.
(81) Bickelhaupt, F. M.; Fokkens, R. H.; de Koning, L. J.; Nibbering, N. M. M.; Baerends, E. J.; Goede, S. J.; Bickelhaupt, F. *Int. J. Mass Spectrom. Ion Processes* **1991**, *103*, 157.
(82) Ziegler, T.; Tschinke, V.; Ursenbach, C. *J. Am. Chem. Soc.* **1987**, *109*, 4825.
(83) Ziegler, T.; Tschinke, V.; Versluis, L.; Baerends, E. J. *Polyhedron* **1988**, *7*, 1625.
(84) Fan, L.; Ziegler, T. *J. Chem. Phys.* **1990**, *92*, 3645.
(85) Fan, L.; Ziegler, T. *J. Am. Chem. Soc.* **1992**, *114*, 10890 and references cited therein.
(86) Ziegler, T. *Chem. Rev.* **1991**, *91*, 651.
(87) Ziegler, T.; Rauk, A. *Theor. Chim. Acta* **1977**, *46*, 1.

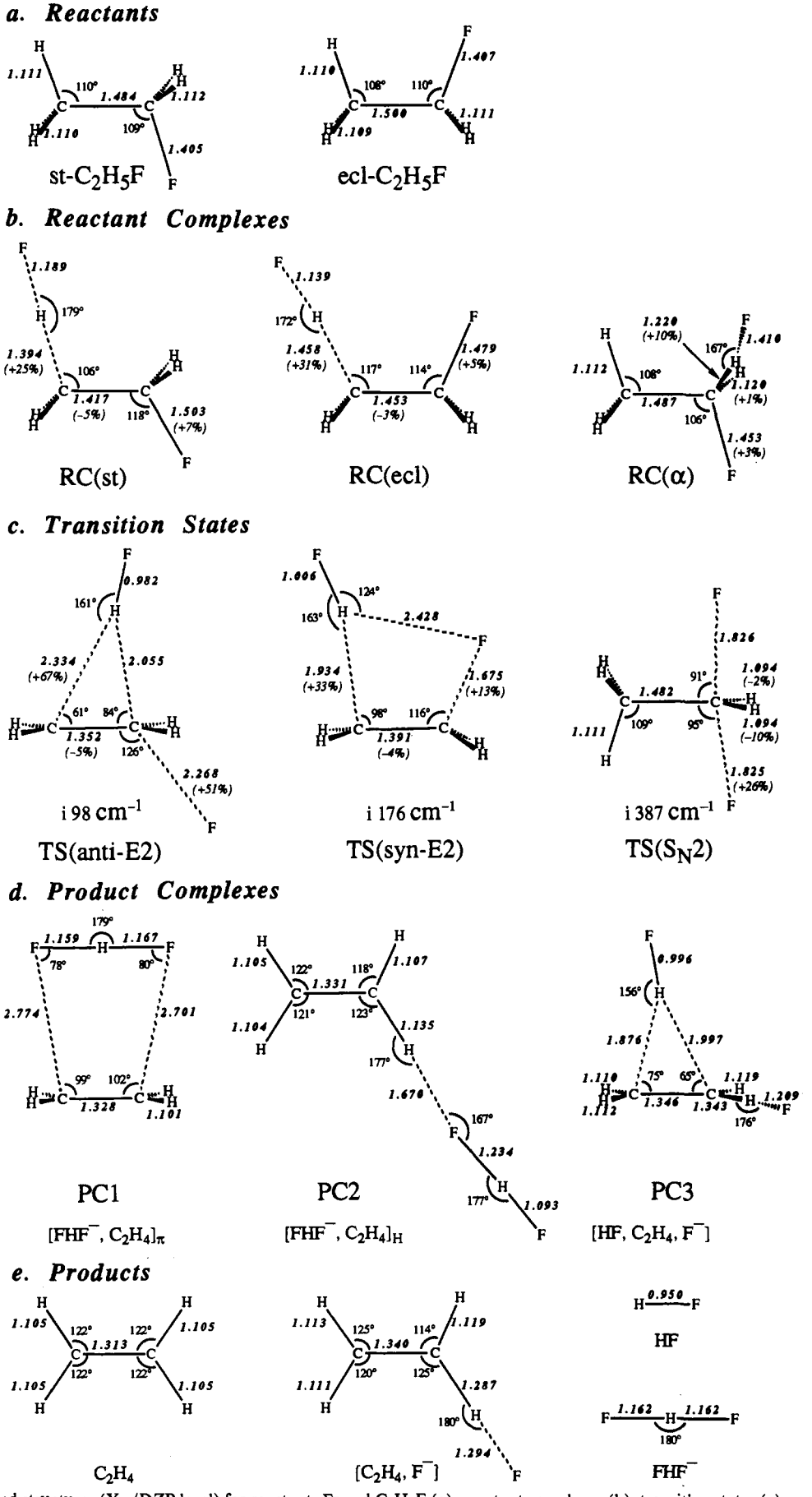

Figure 2. Calculated structures (Xα/DZP level) for reactants F^- and C_2H_5F (a), reactant complexes (b), transition states (c), product complexes (d), and products (e). Bond lengths (Å) are represented in bold/italic. In b and c, the change in the bond length (%) of selected bonds has been displayed for R(st)/R(ecl)/R(st)→RC(st)/RC(ecl)/RC(α) and RC(st)/RC(ecl)/RC(α)→TS(anti-E2)/TS(syn-E2)/TS(S_N2), respectively. In c, furthermore, the imaginary frequencies associated with the transition states have been displayed.

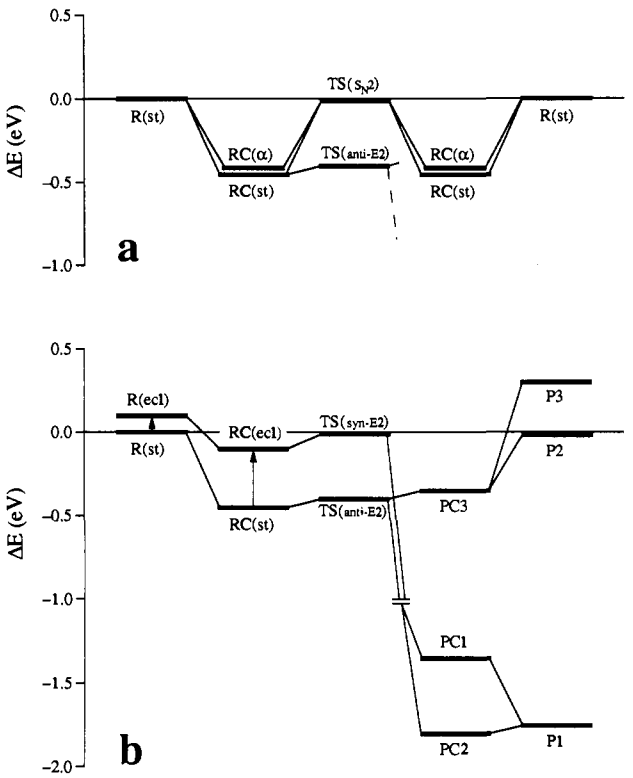

Figure 3. Schematic reaction energy profiles (LDA/NL/TZPP level) for (part of) the anti-E2 together with the S_N2 reaction (a) and the (complete) anti-E2 together with the syn-E2 reaction (b) of F^- and C_2H_5F.

the F^- $2p_z$, and the substrate LUMO, i.e. the st-C_2H_5F 8a′, the latter having σ antibonding character in the C^β–H and the C^α–F bond, and π-bonding character in the C–C bond (*vide infra*). The reactant complex RC(st) seems to be predestined to react further via the TS(anti-E2) (Figure 2), i.e. via the anti-elimination pathway, on the basis of the structural considerations. Nevertheless, in the gas phase, the internal rovibrational energy gained upon complexation of F^- and st-C_2H_5F remains available[32,33] for rearrangement to RC(α), from which the S_N2 process may preferentially proceed. It is interesting to note, however, that preliminary calculations indicate that the F^- is captured only by the C^α–H bond to form RC(α) if it approaches in a relatively narrow cone around the C^α–H axis.

Comparison of the reaction profiles of the anti-E2 and the S_N2 reaction (Figure 3a, Table I) clearly shows that the transition state for the S_N2 substitution (–0.02 eV relative to R(st)) is considerably higher in energy, i.e. 0.39 eV, than that for the anti-E2 elimination (–0.41 eV relative to R(st)). Furthermore, the imaginary frequency associated with the reaction mode of the TS(anti-E2) (*i* 98 cm^{-1}) is considerably lower than that of the TS(S_N2) (*i* 387 cm^{-1}) (Figure 2c). The higher imaginary frequency of the TS(S_N2) corresponds to a "steeper" saddle point on the energy hypersurface and can be associated with a relatively tight transition state, i.e. a transition state with a low density of states and thus a high activation entropy. This is confirmed by the relatively high frequencies of the normal modes of the TS(S_N2) (86, 315, 340, 361 cm^{-1}, etc.) if compared to those of the TS(anti-E2) (33, 83, 131, 169 cm^{-1}, etc.). A relatively tight transition state for the S_N2 substitution is in agreement with the rigid structure of the TS(S_N2), in which bond breaking occurs to a much lesser extent than in the TS(anti-E2): in TS(S_N2), the C^α–F (leaving group) bond has been elongated by only 26%, while the C^α–F (base) bond is already equally strong; in contrast to this, in TS(anti-E2), both the C^β–H (+67%) and the C^α–F (+51%) bond have been expanded considerably, resulting in a relatively loose structure in spite of the formation of the H–F bond (Figure 2c).

Concluding, the base-induced anti-E2 elimination strongly prevails over the S_N2 substitution due to both a lower activation energy and a less negative activation entropy, but also because of the preferential formation of a reaction complex RC(st) which is predetermined to react further via the anti-E2 pathway.

Anti-E2 *versus* Syn-E2. In this subsection, the competition between the base-induced anti-E2 and syn-E2 elimination (Figure 1) of F^- and fluoroethane is discussed. In principle, F^- can also combine with fluoroethane in the eclipsed conformation (F^- + ecl-C_2H_5F, R(ecl)) under formation of the reactant complex RC(ecl), which is 0.35 eV higher in energy than RC(st) (Table I, Figure 3b). In RC(ecl), the C^β–H bond (1.458 Å) and the C^α–F bond (1.479 Å) have been elongated by 31% and 5%, respectively, while the C–C bond (1.453 Å) has been contracted by 3% with respect to the reactant ecl-C_2H_5F (Figure 2). The higher energy of RC(ecl) can be explained only partly by the energy difference of 0.10 eV between ecl-C_2H_5F and st-C_2H_5F. The energy difference between RC(ecl) and RC(st) can be followed in detail through the energy contributions in Table II. It is not due to electrostatic effects (ΔE_{elstat} is equal) but is caused by stronger Pauli repulsion between the base and the fluoroethane occupied orbitals, i.e. between lone pairs of F^- and the F of C_2H_5F, and also between the base HOMO, i.e. the F^- $2p_z$, and the occupied substrate 6a′ (σ bonding for C^β–H). The Pauli repulsion is relieved by a stronger mixing with the ecl-C_2H_5F 8a′ LUMO (*vide infra*), hence more attractive ΔE_{oi}; the larger resulting 8a′ occupation (0.34 *versus* 0.27 electrons in RC(st)) explains the larger extension of the C^β–H in RC(ecl) (+31%) if compared to that in RC(st) (+25%). (Note that such bond elongations raise the energy required to distort C_2H_5F to the geometry it has in RC(ecl), as reflected in a larger ΔE_{prep} that cancels part of the more favorable ΔE_{oi}.) The structural changes upon formation of RC(ecl) indicate the strong tendency of the complex to react further via the syn-E2 pathway. This parallels the behavior of RC(st) in the anti-E2 reaction. However, an important difference between the two reactant complexes is that RC(st) is a real energy minimum, while RC(ecl) represents a "transition state" of rotation around the C–C axis (imaginary frequency *i* 23 cm^{-1}).

Comparison of the reaction profiles of the anti-E2 and the syn-E2 reaction (Figure 3b, Table I) clearly shows that the transition state for the syn-E2 elimination (–0.02 eV relative to R(st)) is considerably higher in energy, i.e. 0.39 eV, than that for the anti-E2 elimination (–0.41 eV relative to R(st)). It is interesting to note, however, that both the anti-E2 and the syn-E2 processes have comparably low energy barriers of 0.05 and 0.09 eV, respectively, with respect to the corresponding reactant complexes (RC(st) and RC(ecl)). Furthermore, the imaginary frequency associated with the reaction mode of the TS(syn-E2) (*i* 176 cm^{-1}) is higher than that of the TS(anti-E2) (*i* 98 cm^{-1}), but lower than that of TS(S_N2) (*i* 387 cm^{-1}). This corresponds to a TS(syn-E2) of intermediate tightness (*vide supra*), as is confirmed by the frequencies of the normal modes (93, 136, 195, 382 cm^{-1}, etc.). The tighter transition state for the syn-E2 elimination is in agreement with the much smaller extent of elongation of the C^β–H (1.934 Å, +33%) and the C^α–F (1.675 Å, +13%) bonds in TS(syn-E2) if compared to TS(anti-E2) (Figure 2c; note that percentages are relative to reactant complexes). It is further noted that (i) dissociation of the C^β–H bond precedes dissociation of the C^α–F bond to a higher extent in TS(syn-E2) and (ii) contraction of the C^α–C^β has occurred to a much lesser extent in TS(syn-E2). It is stressed that the relatively small contractions of C^α–C^β in TS(anti-E2) and TS(syn-E2), respectively, by 0.132 and 0.093 Å with respect to st-C_2H_5F correspond to 77% and 54% of the way from the single bond in st-C_2H_5F (1.484 Å) to the double bond in C_2H_4 (1.313 Å, Figure 2). The structure of TS(anti-E2) is thus more alkene-like, whereas the structure of TS(syn-E2) is more carbanion-like. Therefore, it is concluded that the syn-E2 elimination is more

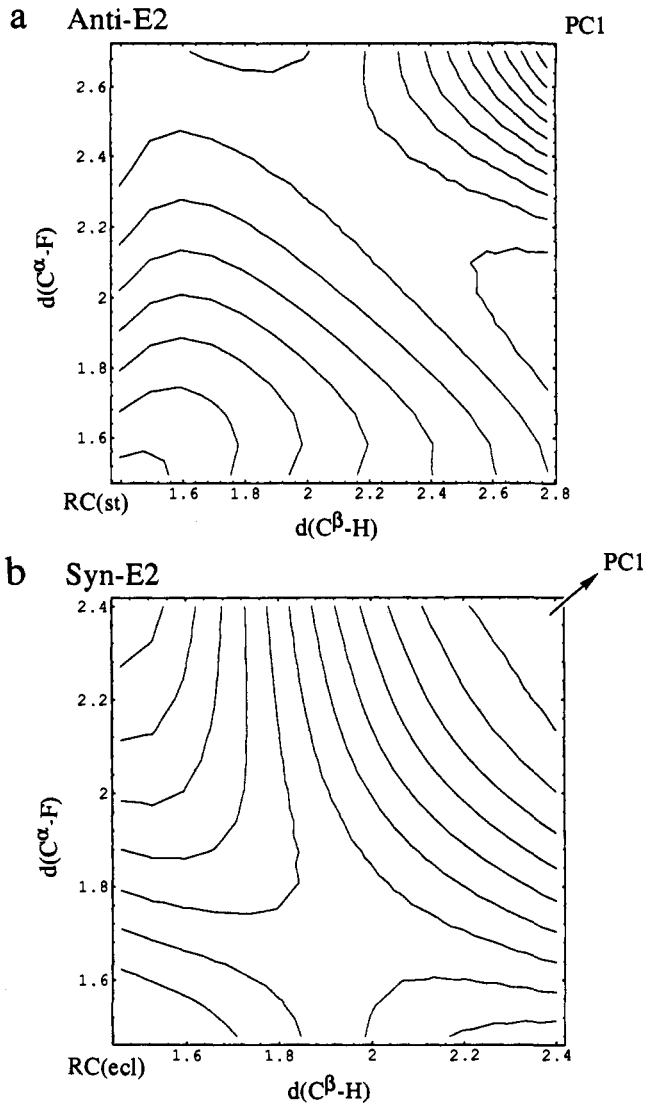

Figure 4. Two-dimensional reaction energy surface $E(d(C^{\beta}\text{–H}), d(C^{\alpha}\text{–F}))$ (Xα/DZP level) for the anti-E2 reaction (a) and the syn-E2 reaction (b) of F^- and C_2H_5F (contour spacing ca. 0.1 eV).

E1cb-like, whereas the anti-E2 elimination is nearly central E2. This is also revealed by the charge distribution (Figure 8). In TS(syn-E2), the C^{β} and C^{α} carry a charge of –0.41 and +0.03 electrons, respectively, reflecting the carbanion character of TS(syn-E2). Differently, in TS(anti-E2), the charge is distributed more homogeneously, amounting to –0.23 electrons on C^{β} and –0.17 electrons on C^{α}; this resembles the situation in C_2H_4, where each carbon atom bears a charge of –0.15 electron. For comparison, in st-C_2H_5F, C^{β} and C^{α} carry a charge of –0.47 and +0.23 electrons, respectively.

The features of the two base-induced elimination reactions are illustrated by the shape of the two-dimensional reaction energy surfaces $E(d(C^{\beta}\text{–H}), d(C^{\alpha}\text{–F}))$ displayed in Figure 4. The more rigid structure of the TS(syn-E2) shows up in a less extended saddle region. The syn-E2 saddle region is reached essentially by "going slightly to the right", i.e. moderate C^{β}–H bond expansion, reflecting some E1cb character of the syn-E2 elimination. Most strikingly, there is no distinct channel on the anti-E2 surface leading directly from the reactant complex to the saddle region. Instead, the system displays a weak tendency to elongate initially either the C^{β}–H or the C^{α}–F bond to some extent, before the other bond is expanded, i.e. there is a weak indication of a E1cb-like and a E1-like channel on the anti-E2 surface. It is concluded that the anti-E2 reaction is virtually ideal E2 with respect to the transition-state geometry but that the reaction path toward this transition state cannot be classified in this way, as there is no clear preference on the very shallow slope of the reaction energy surface.

Anti-E2 and syn-E2 elimination result in the exothermic formation (Figure 3b, Table I) of the same product complex PC1 (–1.36 eV relative to R(st), Figure 2d) under the C_s symmetry constraint used in the calculation of the reaction energy surface (Figure 4). PC1 is composed of FHF^- and C_2H_4 and can decompose to the separated products P1 (–1.75 eV relative to R(st), Figure 2e) either directly or via rearrangement to the more stable PC2 (–1.78 eV relative to R(st)) in which FHF^- hydrogen bonds to a C–H bond of ethene. Conceivably, release of the C_s constraint may open the possibility in the *anti*-E2 elimination to lead to the production of the relatively unstable PC3 (–0.37 eV relative to R(st), Figure 2d). The product complex PC3 is composed of rather weakly interacting HF, C_2H_4, and F^- and may decompose via rearrangement to the more stable PC2. Alternatively, PC3 can separate either partly to HF and the ion/molecule complex [C_2H_4, F^-], i.e. the products P2 (–0.02 eV relative to R(st)), or completely to the products P3 (+0.29 eV relative to R(st)). In principle, the endothermic reaction channel toward P3 is not available under low-pressure conditions in the gas phase.[32,33]

Concluding, the base-induced anti-E2 elimination strongly prevails over the syn-E2 elimination due to both a lower activation energy and a less negative activation entropy, but also because the syn-E2 reactant complex represents a labile structure which tends to rotate around the C–C bond, away from the reactive conformation. Both anti- and syn-E2 reactions preferentially result in the formation of FHF^- and C_2H_4.

The Electronic Structure of the Substrate. At this point, we perform a detailed analysis of the electronic structure of the fluoroethane substrate. To this end, C_2H_5F is built up from the well-known methyl radicals $CH_3^{\bullet}$ and $CH_2F^{\bullet}$.[72] The corresponding qualitative MO interaction diagram as inferred from our calculations is depicted in Scheme I. For simplicity, only MO levels of A' symmetry have been drawn (Note, however, that the A'' methyl orbitals have been drawn within parentheses.) The MO interaction diagram for the related but less complicated ethane (C_2H_6), composed of two $CH_3^{\bullet}$ radicals, has been included in Scheme I for comparison. The occupied spectrum of the $CH_3^{\bullet}$ radicals is composed of a carbon 2s/hydrogen 1s bonding σ MO (σ bonding between C and H_3), a degenerate carbon 2p/hydrogen 1s bonding π MO (π bonding between C and H_3), and a carbon (2s + 2p) nonbonding n_C SOMO. The two lowest virtual $CH_3^{\bullet}$ orbitals are the σ^* LUMO and the π^*, i.e. the C/H_3 antibonding counterparts of the σ and π orbitals. The C–C bond between the methyl radicals in C_2H_6 is provided by the strong (n_C + n_C) electron pair bond which has a highly energetic antibonding counterpart in the virtual spectrum. The LUMO of C_2H_6 is given by the bonding (σ^* + σ^*) combination of the $CH_3^{\bullet}$ LUMOs. The σ/σ and π/π closed-shell interactions between the methyl radicals result in Pauli repulsion.

The electronic structure of C_2H_5F is comparable to that of C_2H_6, to a certain degree. Note, that in the σ, π, σ^*, and π^* orbitals of $CH_2F^{\bullet}$ the fluorine 2p pointing to the carbon atom plays the role of the hydrogen 1s orbital. The fluorine 2s has a very low energy and, essentially, does not interact with other AOs. So the main differences between $CH_2F^{\bullet}$ and $CH_3^{\bullet}$ are the two fluorine 2p orbitals perpendicular to the C–F bond. They mix only very weakly with other AOs in $CH_2F^{\bullet}$ and provide the fluorine nonbonding n_F lone pairs. The C–C bond between $CH_3^{\bullet}$ and $CH_2F^{\bullet}$ in fluoroethane is provided by a strong (n_C + n_C) pair bond. The antibonding counterpart in the virtual spectrum is highly energetic, and it is stressed that it does not represent the fluoroethane LUMO. Instead, the LUMO is given by the bonding combination of the $CH_3^{\bullet}$ σ^* and π^* with the $CH_2F^{\bullet}$ π^*. This will turn out to be of crucial importance for the understanding

Scheme I

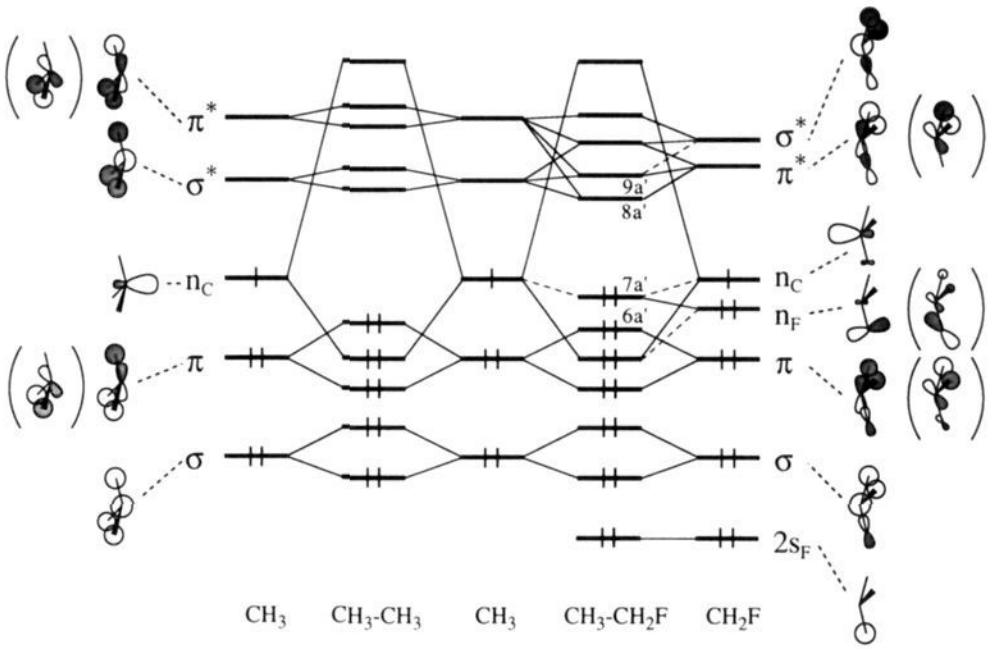

of the reactivity of the substrate (*vide infra*). The somewhat more complex interactions in the virtual spectrum of C_2H_5F are the result of the reversed order of the $CH_2F^\bullet$ σ^* and π^*, if compared to $CH_3^\bullet$ (see also Scheme III). In C_2H_5F, the $CH_2F^\bullet$ n_F lone pair of *A'* symmetry has some repulsive interaction with the $CH_3^\bullet$ n_C SOMO (Scheme I).

Orbital Interactions and the Catalytic Effect of the Base. In this subsection, the magnitude and the origin of the catalytic effect of the base in the anti- and syn-E2 eliminations are investigated. In particular, the question is addressed as to why the transition state is selectively stabilized and why this stabilization is more effective for the anti elimination. To this end, we consider the thermal, that is the uncatalyzed syn and anti elimination (E) of HF from fluoroethane (eq 2). The structures

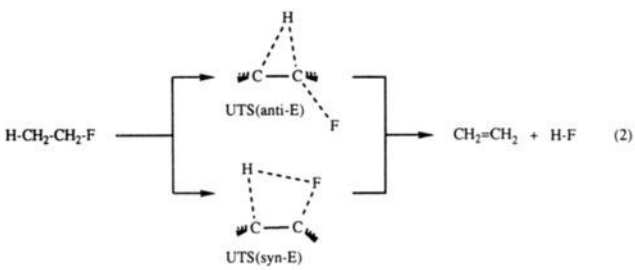

of the TS(anti-E2) and TS(syn-E2) (Figure 2c) with the base F^- removed serve as model systems for the uncatalyzed transition states UTS(anti-E) and UTS(syn-E), respectively. Although artificial to some extent, this choice is plausible and, moreover, allows one to couple the energetics of catalysis with a qualitative picture based on an analysis of the base/substrate interaction in the E2 transition states (Table II). Furthermore, the syn-E barrier of 3.60 eV calculated for our model transition state (Table I) is in reasonable agreement with the SCF/4-31G and CI-SD+QC/4-31G values obtained by Kato and Morokuma,[88] which are lower by 10% and 17%, respectively. In addition, the structure of our UTS(syn-E) is qualitatively analogous to the SCF/4-31G-optimized structure,[88] in spite of some quantitative differences (e.g. a much longer H–F distance).

In Figure 5, the energetics of the base-catalyzed and the uncatalyzed elimination reactions are displayed. In the absence

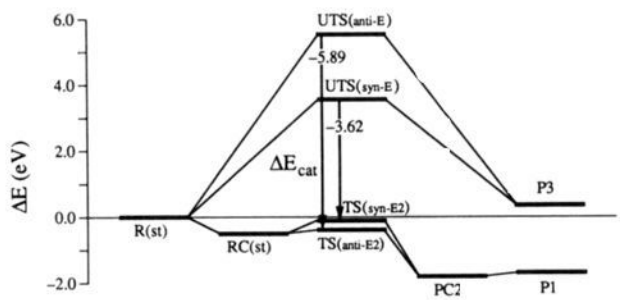

Figure 5. Catalytic effect of the base F^- on the 1,2-elimination of HF from C_2H_5F (LDA/NL/TZPP energy profile).

of the F^- catalyst, the anti (+5.48 eV) as well as the syn elimination (+3.60 eV) of HF from fluoroethane suffers from an enormous activation barrier (Figure 5, Table I). As one might expect intuitively, the uncatalyzed syn-E reaction proceeds via a lower energetic transition state due to the onset of a favorable H/F interaction in an early stage of the reaction, associated with a smaller extent of deformation.

The high activation energy reflects the symmetry-forbidden character of these thermic 1,2-eliminations. This is illustrated in Scheme II by the qualitative MO interaction diagrams inferred from our calculations for the syn elimination of HF from C_2H_5F (right hand side) and for the analogous but less complicated syn elimination of H_2 from C_2H_6 (left hand side). Again C_2H_6 and C_2H_5F are built up from two methyl radicals, i.e. $CH_3^\bullet + CH_3^\bullet$ and $CH_3^\bullet + CH_2F^\bullet$, respectively.

First, the simple case of the H_2 elimination from C_2H_6 is considered (Scheme II, left hand side). Upon elongation of the C–H bond, the $CH_3^\bullet$ π orbital rises while the π^* orbital decreases in energy, effectively crosses the σ^*, and thus, becomes the LUMO of the $CH_3^\bullet$ fragment. At first, the HOMO of C_2H_6 is provided by the $(\pi - \pi)$ combination, which is C–C π antibonding, C–H σ bonding, and H–H σ antibonding. The LUMO is given by the $(\pi^* + \pi^*)$ combination, which is C–C π bonding, C–H σ antibonding, and H–H σ bonding. Upon further elongation of the C–H bonds, the $(\pi^* + \pi^*)$ and $(\pi - \pi)$ MOs interchange their relative energetic order and electron occupation, i.e. the transition state for the symmetry-forbidden reaction is passed, and the system changes from an ethane (C_2H_6) to an ethene + molecular hydrogen ($C_2H_4 + H_2$) electronic configuration. In the limit of infinite

(88) Kato, S.; Morokuma, K. *J. Chem. Phys.* **1980**, *73*, 3900.

Scheme II

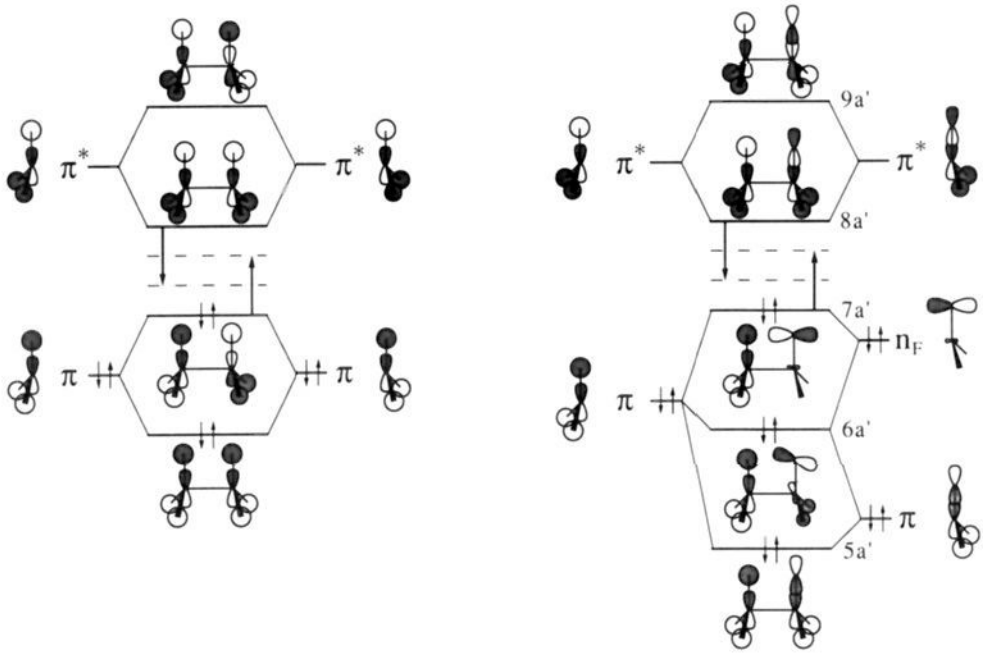

separation of C_2H_4 and H_2, the ($\pi^* + \pi^*$) HOMO and the ($\pi - \pi$) LUMO develop toward the C–C π and the C–C π^*, respectively, of ethene, whereas the ($\pi + \pi$) and ($\pi^* - \pi^*$) combinations transform into the H–H σ and σ^* orbitals of molecular hydrogen.

For the thermic syn elimination of HF from C_2H_5F, the situation is similar in the sense that a HOMO/LUMO crossing occurs, which is characteristic for a symmetry-forbidden reaction. Differences arise from the presence of the n_F lone pair on $CH_2F^\bullet$ and because of the nodal structure of the $2p_F$ AO in the π^* and σ^* orbitals of $CH_2F^\bullet$ (Scheme II, right hand side). In eclipsed C_2H_5F, this n_F lone pair has a strong interaction with the π orbital of $CH_3^\bullet$, mainly due to the $CH_3^\bullet/CH_2F^\bullet$ $1s_H/2p_F$ overlap (see also the corresponding contour plots of the ecl-C_2H_5F 6a′ and 7a′ orbitals in Figure 7b). At first, therefore, the HOMO of eclipsed C_2H_5F is provided by the $CH_3^\bullet/CH_2F^\bullet$ ($\pi - n_F$) combination, which is C–C and C–F nonbonding, C–H σ bonding, and H–F σ antibonding. The LUMO is given by the ($\pi^* + \pi^*$) combination, which is C–C π bonding, C–H and C–F σ antibonding, and H–F *non*bonding (due to the fluorine 2p nodal surface in the $CH_2F^\bullet$ π^* orbital). Upon further elongation of the C–H and C–F bonds, the ($\pi^* + \pi^*$) and ($\pi - n_F$) MOs interchange their relative energetic order and electron occupation, i.e. the transition state for the symmetry-forbidden reaction is passed, and the system changes from a fluoroethane (C_2H_5F) to an ethene + hydrogen fluoride (C_2H_4 + HF) electronic configuration. In the limit of infinite separation of C_2H_4 and HF, the ($\pi + n_F$) orbital 6a′, the ($\pi^* + \pi^*$) "HOMO" 8a′ and the ($\pi - n_F$) "LUMO" 7a′ develop toward the H–F σ orbital, a fluorine lone pair, and the H–F σ^* orbital, respectively, of hydrogen fluoride, whereas the ($\pi + \pi$) (5a′) and ($\pi^* - \pi^*$) combinations transform into the C–C π and π^* orbitals of ethene. Note that the 5a′ and 8a′ orbitals may be looked upon as bonding and antibonding combinations, respectively, of the C–C π with a H–F nonbonding orbital. The C–C π-bonding character is clearly visible in the plots of 8a′ in both the staggered (Figure 6a) and eclipsed (Figure 7a) conformations. Occupation of the 8a′ upon passing the transition state implies that the C–C π bond fully develops; the antibonding with HF in the 8a′ causes HF to be expelled and all of the C–C π-bonding character to revert to the 5a′.

Introduction of the base results in selective stabilization of the transition states (Figure 5, Table I). The catalytic effect for the anti elimination (–5.89 eV at the LDA/NL/TZPP level, –6.36 eV at the LDA/NL/DZP level; see Table II) is considerably higher than that for the syn elimination (–3.62 eV at the TZPP, –4.28 eV at the DZP). This leads to an inversion of the energetic ordering of transition states, resulting in an energetically favored base-catalyzed *anti*-E2 reaction.

The mechanism of stabilization of the transition state and the high degree of anti/syn selectivity of the E2 catalyst, i.e. the F^- base, is revealed by a detailed analysis of the electronic structure

Table II. Analysis of the Bonding Mechanism between F^- and the C_2H_5F Fragment in the Reaction Systems RC(st), TS(anti-E2), RC(ecl), and TS(syn-E2) (1 eV = 23.06 kcal/mol)[a,b]

	RC(st)	TS(anti-E2)	RC(ecl)	TS(syn-E2)
		Overlaps $\langle F^- \mid C_2H_5F \rangle$[c]		
$\langle 2p_z \mid 5a' \rangle$	0.08	0.22	0.06	0.08
$\langle 2p_z \mid 6a' \rangle$	0.22	0.16	0.23	0.16
$\langle 2p_z \mid 7a' \rangle$	0.05	0.01	0.06	0.21
$\langle 2p_z \mid 8a' \rangle$	0.19	0.26	0.20	0.24
$\langle 2p_z \mid 9a' \rangle$	0.01	0.05	0.03	0.04
		Populations[d] (electrons)		
$P(2p_z)$	1.77	1.62	1.74	1.65
$P(5a')$	1.99	1.85	1.99	1.99
$P(6a')$	1.88	1.65	1.86	1.91
$P(7a')$	1.99	1.99	1.99	1.78
$P(8a')$	0.27	0.76	0.34	0.56
$P(9a')$	0.02	0.02	0.00	0.00
		Energies[e] (eV)		
ΔE_{elstat}	–2.98	–5.38	–2.98	–4.18
ΔE_{Pauli}	4.65	7.06	5.21	6.87
$\Delta E°$	1.67	1.68	2.23	2.69
ΔE_{oi}	–3.71	–8.04	–4.34	–6.97
ΔE_{int}	–2.04	–6.36	–2.11	–4.28
ΔE_{prep}	0.86	5.51	1.24	3.53
ΔE	–1.18	–0.85	–0.87	–0.75

[a] Calculated at the LDA/NL/DZP level for Xα/DZP geometries (see the Method). [b] See Figure 2 for structures. [c] The fluorine z-axis points to the β-hydrogen of the C_2H_5F fragment. [d] $P(\varphi)$ is the gross Mulliken population that the fragment orbital φ acquires in the complex. [e] $\Delta E°$ is the steric repulsion that comprises both the four-electron destabilizing interactions between occupied orbitals (Pauli repulsion: ΔE_{Pauli}) and the classical electrostatic interaction (ΔE_{elstat}) between the electronic and nuclear charge distributions of the fragments. ΔE_{oi} is the orbital interaction, which comes for more than 90% from the A' symmetry. ΔE_{prep} is the energy required to prepare the C_2H_5F fragment in the geometry that it has in the complex from the free, staggered fluoroethane.

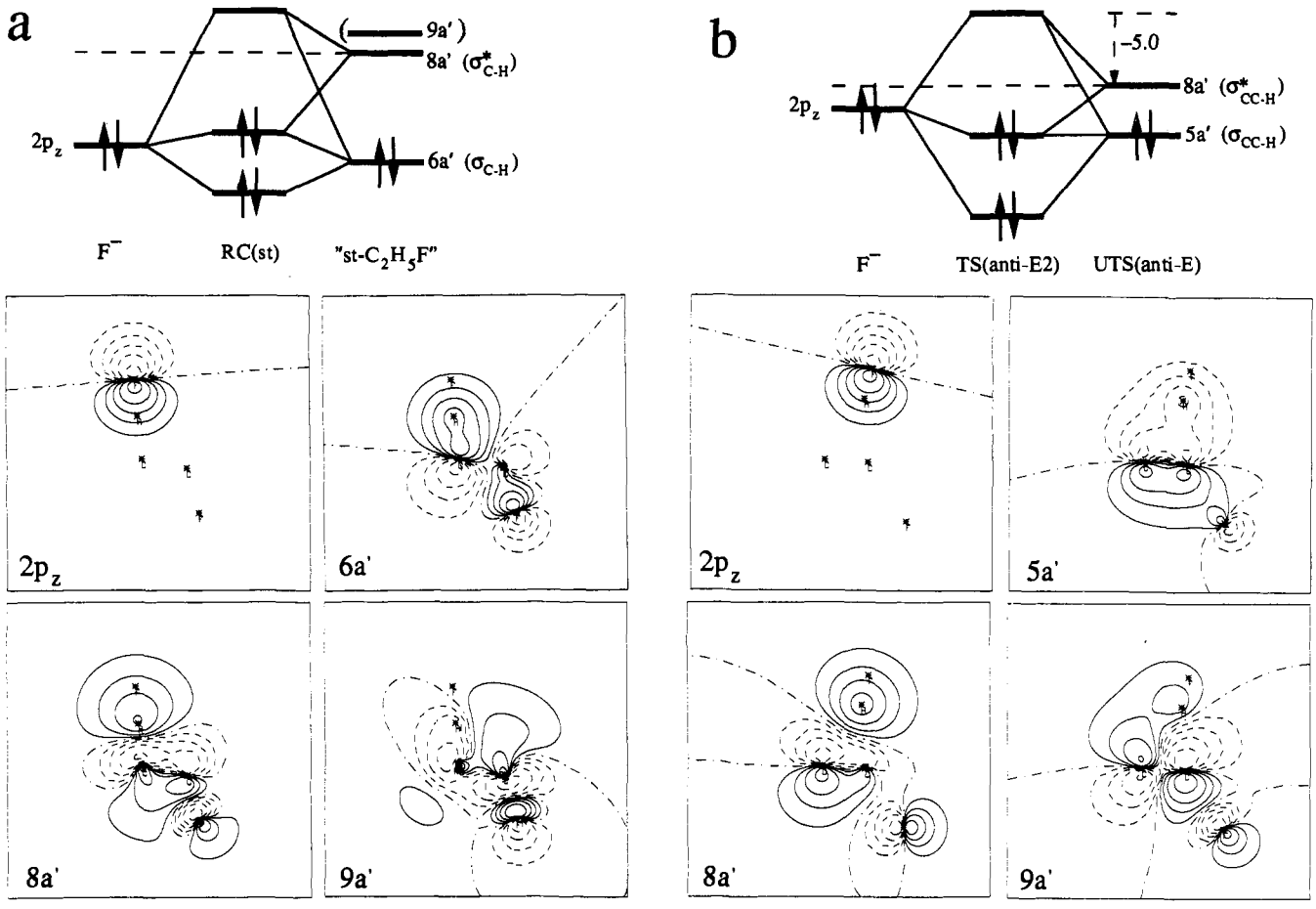

Figure 6. F^-/C_2H_5F MO interaction scheme and contour plots of selected fragment orbitals for anti-E2 reaction systems RC(st) (a) and TS(anti-E2) (b). In b, the stabilization (eV) of the C_2H_5F 8a' is indicated when going from RC(st) to TS(anti-E2). Note that in the fragment orbital plots also the positions of the nuclei of the other fragment are indicated.

of and the interaction between the reactants in the E2 reaction complexes and transition states (see Table II, Scheme I, and Figures 6 and 7). First, the reactant complexes are reviewed in more detail. In both RC(st) (Figure 6a) and RC(ecl) (Figure 7a), the F^- $2p_z$ (base HOMO) interacts with the 6a' (substrate σ_{C-H}) and the 8a' (substrate σ^*_{C-H} and LUMO) (see also Scheme III, left). The interaction between the occupied $2p_z$ and 6a' leads to Pauli repulsion, which is relieved by the mixing of the $2p_z$–6a' combination with the 8a'. This results in a donor/acceptor interaction between the F^- $2p_z$ and the C_2H_5F 8a' and charge transfer within the substrate from the 6a' to the 8a', as reflected in the P(6a') of 1.88 electrons and P(8a') of 0.27 electrons in Table II. The C^β–H and C^α–F bonds are weakened and expand while the C–C bond contracts, mainly due to the donation of charge into the 8a' (strongly σ antibonding for C^β–H, σ antibonding for C^α–F, and π bonding for C–C), but also because of the depopulation of the 6a' (σ bonding for C^β–H and C^α–F and π antibonding for C–C) (see figures 6a and 7a and Scheme I as well as Scheme III, left). The difference between RC(st) and RC(ecl) has already been discussed in the subsection Anti-E2 versus Syn-E2.

Next, the transition states are examined. Extension of the C^β–H and C^α–F bonds in both eclipsed and staggered fluoroethane will of course raise the energy, as reflected in a rise in energy of the occupied orbitals representing these bonds. The important difference introduced by the presence of the base is that the concomitant decrease in energy of the 8a' LUMO now has energetic consequences: the donor/acceptor interaction with the base HOMO becomes much stronger (cf. the large increase in P(8a') in going to the TS, Table II), lowering the energy by as much as 8.04 (anti) and 6.97 eV(syn). In eclipsed fluoroethane, approach of the H^β and leaving group F, which raises the 7a' energy, is facilitated by a favorable, i.e. bonding, interaction between the H and the F. This is reflected by the H–F (1s + 2p) bonding character of the 6a' orbital, which slightly increases when going from ecl-C_2H_5F (in the geometry of RC(ecl)) to UTS-(syn-E) (in the geometry of TS(syn-E2)) (Figure 7b, see also Scheme II). Note, that the occupied 7a' (H–F (1s – 2p) antibonding) and 8a' LUMOs (H–F nonbonding and C–C π bonding) of the TS(syn-E) still have to interchange their energetic order and occupation before a proper ethene + HF configuration is achieved (see also Scheme II). At that point, the base can enter a donor/acceptor interaction with the 7a', which is developing into the HF σ^*. The presence of the base does not lift the symmetry-forbidden character of the reaction but very much alleviates the process.

A favorable H–F interaction in an early stage of C^β–H and C^α–F expansion is inherently impossible for the anti elimination, and the transition state is reached at a point where the C^β–H and C^α–F bonds have been extended to a much higher degree. According to Table II, the energetic cost ΔE_{prep} of reaching the TS geometry (in the absence of the base) is indeed 2 eV higher than for the eclipsed case. There are two factors that make the base catalysis however more effective now (see Figure 5). First, the energy level of the acceptor orbital of C_2H_5F, i.e. the 8a' LUMO, decreases much more for the anti elimination (–5.0 eV) than for the syn elimination (–2.7 eV) when proceeding from the reactant complex geometry to the transition state (Figures 6b and 7b). This has the important consequence that the 8a' LUMO of the UTS(anti-E) is much lower in energy and, hence, is a better partner in the donor/acceptor interaction with the $2p_z$ HOMO of the F^- base. The 8a' population is considerably larger (0.76 electrons *versus* 0.56) and ΔE_{oi} is accordingly more stabilizing (by 1.1 eV). [There are more electronic structure

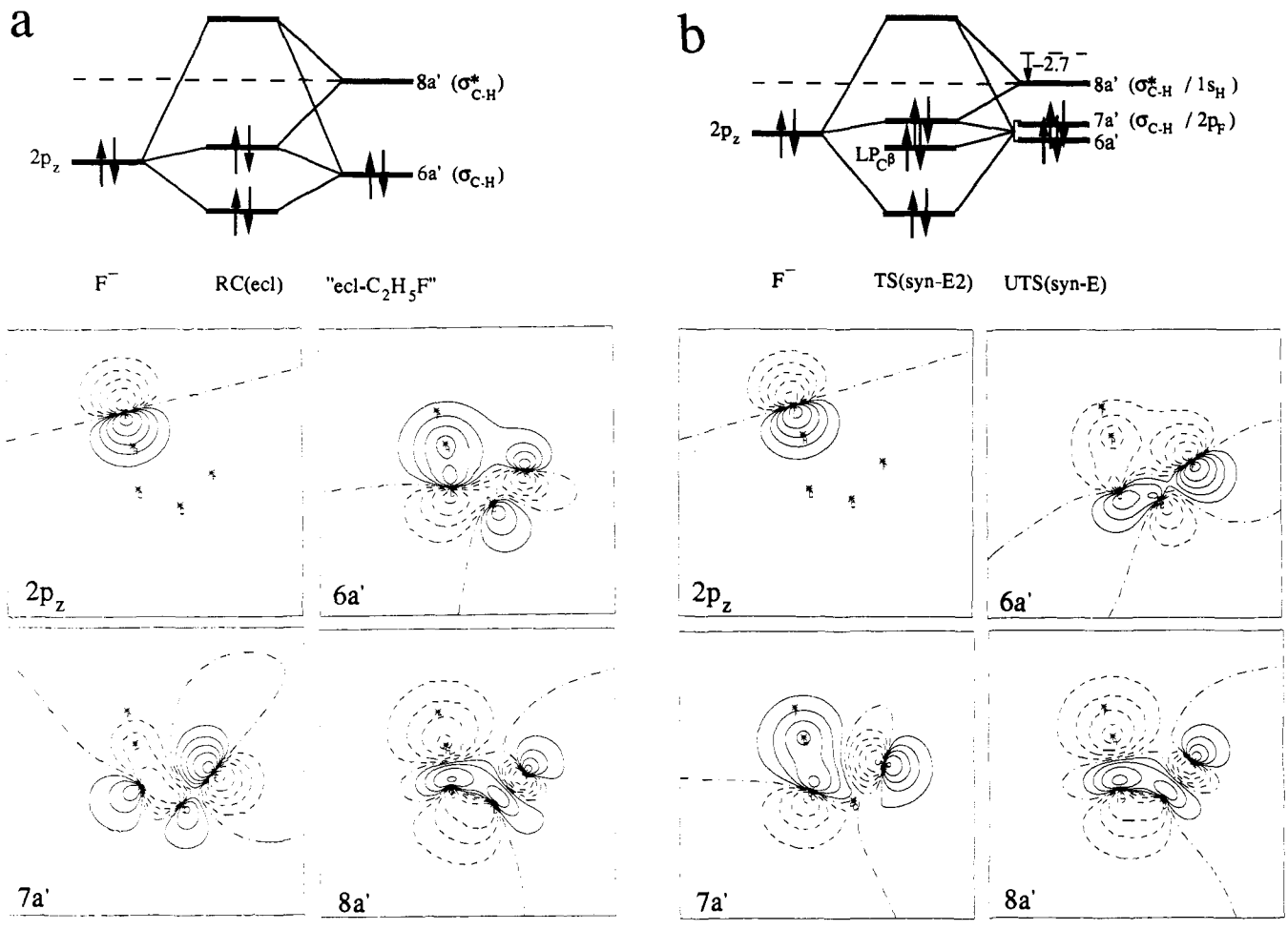

Figure 7. F^-/C_2H_5F MO interaction scheme and contour plots of selected fragment orbitals for syn-E2 reaction systems RC(ecl) (a) and TS(syn-E2) (b). In b, the stabilization (eV) of the C_2H_5F 8a′ is indicated when going from RC(ecl) to TS(syn-E2). Note that in the fragment orbital plots also the positions of the nuclei of the other fragment are indicated.

effects related to the larger geometric distortion of the fluoroethane substrate, such as stronger polarization of the fluoroethane substrate by F^-, as evidenced by the lowering of the 6a′ and 5a′ populations; these are not further detailed here.] Second, the electrostatic stabilization upon approach of the F^- catalyst is also much larger (by 1.2 eV) for UTS(anti-E) than for UTS(syn-E) (compare the ΔE_{elstat} of TS(anti-E2) and TS(syn-E2) in Table II). This reflects the favorable orientation of the dipole moment in UTS(anti-E) for interaction with the F^- base in TS(anti-E2). The pronounced shift of the abstracted proton from the C^β to the C^α position in the TS(anti-E2) (Figure 2c) can be ascribed to a favorable interaction between the H–F moiety and the C_2H_4 π system as well as the negatively charged leaving group.

Concluding, the syn mechanism would prevail in the thermal, i.e. uncatalyzed, elimination of HF from fluoroethane, but a very high barrier precludes this reaction. Preferential stabilization of the loose, highly unsaturated anti-E transition state upon base catalysis reverses this order and makes the anti mechanism the preferred one for the base-induced elimination. The stabilization has a charge transfer (donor/acceptor) as well as an electrostatic nature.

Orbital Interactions and the Competition between E2 and S_N2. In this subsection, a qualitative MO theoretical analysis is given, which enables one to understand and predict which reaction, E2 or S_N2, dominates for a given general substrate C_2H_5L. To this end, a more detailed analysis of the virtual spectrum, in particular of the LUMO of the staggered C_2H_5F substrate, has been performed, where again C_2H_5F is built up from the well-known methyl radicals $CH_3^\bullet$ and $CH_2F^\bullet$.[72] The corresponding qualitative MO interaction diagram as inferred from our calculations is shown at the left hand side of Scheme III.

It appears that the σ^* and π^* orbitals of the $CH_3^\bullet$ fragment are mixed to some extent, especially when the C–H bond is extended as is the case in the reaction complex of F^- and C_2H_5F (see Figure 2). Therefore, both the σ^* and π^* orbitals of $CH_3^\bullet$ mix in a bonding fashion with the $CH_2F^\bullet$ π^* via their carbon 2p character. The resulting fluoroethane 8a′ LUMO has more amplitude at the CH_3 side of the substrate, as the $CH_3^\bullet$ σ^* is lower in energy than the $CH_2F^\bullet$ π^* orbital (Scheme III, left hand side). In this LUMO, the $2p_C$ contribution and the $1s_H$ contribution of the partly removed antihydrogen of CH_3– are amplified, whereas the $2s_C$ contribution and the $1s_H$ contribution of the two gauche hydrogens cancel. The picture in Scheme III highlights the features of the 8a′ LUMO that make its role, discussed in the previous subsection, so important: an extended lobe on the β-hydrogen, *highly* C^β–H σ antibonding, C–C π bonding, and C^α–F σ antibonding (see also Figure 6a). In general, we expect this kind of LUMO for a substrate CH_3CH_2L in which the $CH_2L^\bullet$ π^* orbital is higher in energy than the $CH_3^\bullet$ σ^*. Donor/acceptor interaction of the HOMO of a base B^- with such a LUMO preferentially leads to attack at the β-hydrogen and to C^β–H bond elongation, which is the onset to the E2 reaction (Scheme III, left hand side). Note that this character of the LUMO also explains the coplanarity of the reaction, i.e. preferential attack on the antihydrogen of the CH_3–rather than on gauche hydrogens. If we would rotate the CH_2L– over 180° around the C–C axis, so as to position the leaving group L syn with respect to H^β, it is clear that the interactions would be similar,

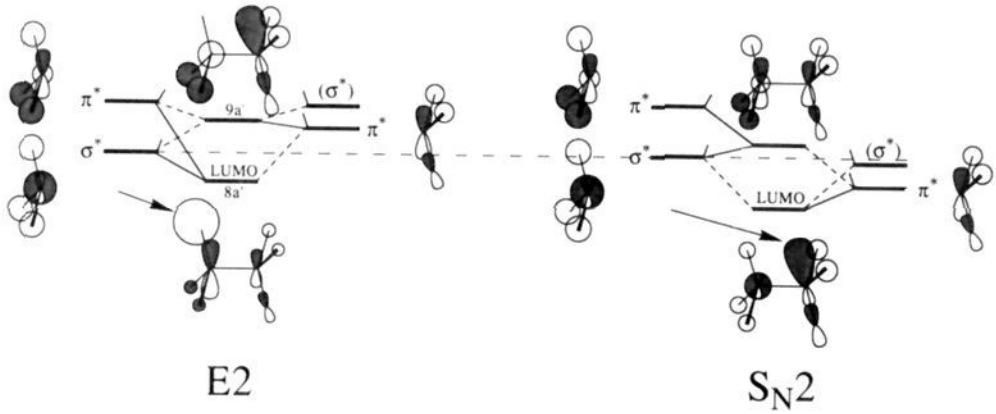

Figure 8. Gross Mulliken atom charges (in electrons; LDA/NL/DZP level) for the E2 and S_N2 transition states.

Scheme III

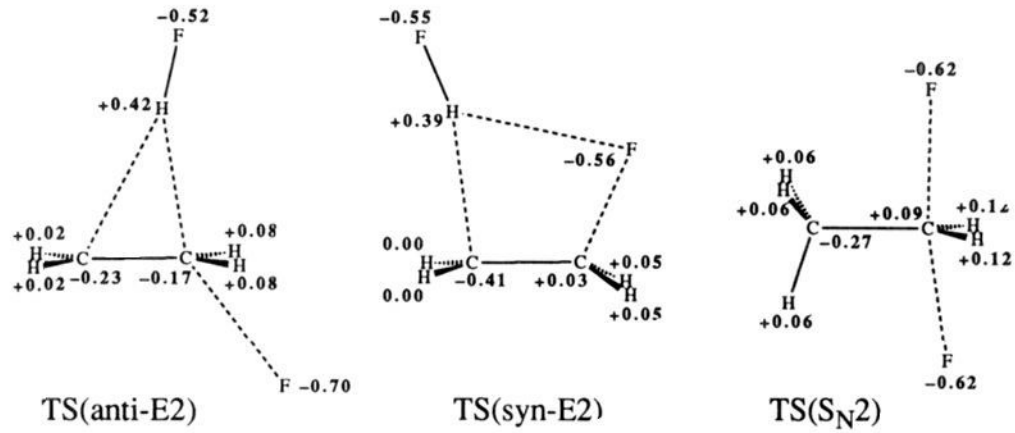

giving rise to large syn H^β amplitude and small amplitude on the other hydrogens. "Orbital control" is thus clearly anti- or syn-coplanar directing.

The 9a′ LUMO+1 (see Scheme III, left, and Figure 6a) has a suitable shape for attack at the C^α, leading to the S_N2 reaction. Such an orbital can become the LUMO if the energy of the C–L antibonding $CH_2L^\bullet$ π^* orbital decreases when the $\langle 2p_{C^\alpha}|np_L\rangle$ overlap becomes smaller, for example due to a longer and weaker C–L bond. This leads to a decrease of the energy of the substrate C_2H_5L LUMO. As a result, the donor/acceptor interaction with the base HOMO and, therefore, the E2 reaction are enhanced (*vide supra*). However, when the energy of the $CH_2L^\bullet$ π^* orbital falls below that of the $CH_3^\bullet$ σ^*, the interaction with $CH_3^\bullet$ π^* diminishes and the somewhat weak interaction with the $CH_3^\bullet$ σ^* remains: the LUMO acquires more amplitude on the CH_2L side of the substrate. Furthermore, there is also admixture of $CH_2L^\bullet$ σ^* character and, as a result, the LUMO has an extended lobe at the "backside" of the $-CH_2L$ group and has predominantly C^α–L antibonding character. Donor/acceptor interaction of the HOMO of a base B^- with such a LUMO preferentially leads to a "backside attack" at the C^α–L bond and to C^α–L bond elongation, which is the onset to the S_N2 reaction (Scheme III, right hand side).

It is emphasized that for a given substrate the electronic structure of the base should determine the E2 *versus* S_N2 selectivity. Inspection of Figure 6a reveals that the C^α–L backside lobe of the 9a′ LUMO+1 of st-C_2H_5F is slightly more extended and less intense than the β-hydrogen lobe of the 8a′ LUMO. A base with a diffuse HOMO should thus have a more favorable overlap and interaction with this diffuse backside lobe of the substrate 9a′ LUMO+1 than a base with a compact HOMO, which in turn should have a larger overlap and interaction with the β-hydrogen lobe of the substrate 8a′ LUMO. Therefore, the S_N2 pathway is expected to become more accessible for bases with a diffuse nucleophilic center, whereas bases with compact nucleophilic centers are expected to react preferentially via the E2 pathway.

The E2H and E2H/E2C Spectra. The base-induced syn-E2 elimination of F^- and fluoroethane proceeds via a E1cb-like transition state, as is apparent from the stronger elongation of the C^β–H bond relative to the elongation of the C^α–F bond (Figure 2), the anti elimination being more central E2. Consequently, the syn-E2 transition state has a much more pronounced charge development on the C^β (–0.41 electrons) than on the anti-E2 transition state (–0.23 electrons; Figure 8). The 1,2-shift of the HF moiety from the C^β to the C^α is an important feature of the TS(anti-E2) which is not accounted for in the formalism of the E2H spectrum.

There is no indication for an E2C-like interaction, i.e. a (weak) covalent interaction of the base with the C^α–F bond. In the reactant complex RC(st), the base $2p_z$ has a very poor overlap of 0.01 with the "backside" lobe of the substrate 9a′, which is the σ^*_{C-F} acceptor in the S_N2 reaction and is calculated to be 1.4 eV above the 8a′ LUMO (Figure 6a, Table II). This trend continues for the TS(anti-E2), where $\langle 2p_z|9a'\rangle$ is only slightly larger and amounts to 0.05 (Figure 6b, Table II). As a result, there is no donor/acceptor interaction with the 9a′, and P(9a′) amounts to only 0.02 electrons in both the RC(st) and the TS(anti-E2) (Table II). For comparison, the calculations reveal that in the transition state for S_N2 substitution the F^- $2p_z$ has an overlap of 0.18 with the "backside" lobe of the substrate σ^*_{C-F} acceptor orbital, which now is populated by 0.33 electrons. The absence of E2C-like interactions is in agreement with the "E2H nature" of the fluoroethane 8a′ LUMO (see Scheme III, left, and Figure 6a) and the related strong preference of the anti-E2 over the S_N2 reaction.

Comparison with Previous Studies. It appears from our results that the C^β–H and the C^α–F bonds expand considerably upon

formation of the reactant complexes for elimination, mainly due to charge donation of the base into the delocalized 8a′ LUMO of the substrate C_2H_5F (Figures 6a and 7a). This nicely confirms the concept of "electronic coupling" between the C^β–H and the C^α–F bonds, already employed by Fukui et al.[49,50] We have found this donor/acceptor interaction between the base HOMO (F^- $2p_z$) and the 8a′ LUMO of the C_2H_5F fragment to play a key role in the selective stabilization of the transition state for anti elimination, in addition to an important electrostatic factor. This picture of selective catalysis principally differs from the one developed by Bach et al.[54] In their conception,[54] the elimination is conceived as an internal S_N2 reaction in which the developing C^β lone pair (or the C^β–H electron pair) performs a backside attack on the σ^*_{C-F} orbital. Accordingly, the syn elimination is hampered by the need of an inversion of the configuration at the C^β center, in order to enable the C^β lone pair to interact with the σ^*_{C-F} orbital. The simplicity of this view is tempting at first sight. However, it is not corroborated by our results, which single out the interaction with the attacking base as providing the essential stabilization. Furthermore, the inversion of configuration at C^β in the TS(syn-E2) is not observed in our calculations (Figure 2c; the dihedral angle $HC^\beta C^\alpha$(HF) amounts to 96°, where the first H refers to a C^β-bonded hydrogen atom and the second H refers to the F^- base-bonded proton).

Theoretical investigations on the prevalence of E2 over S_N2 reactions in the gas phase have also been performed for the F^-/C_2H_5F model system by Minato and Yamabe at various levels of conventional *ab initio* theory.[55,56] They conclude that preferentially the reactant complex for anti-E2 elimination is formed.[55] Furthermore, they arrive at a more favorable, i.e. less negative, activation entropy for the anti-E2 reaction, if compared to the S_N2 reaction.[55] These results are in nice agreement with our findings. Minato and Yamabe[55,56] also arrive at similar trends in structural reorganization upon formation of reaction complexes and transition states, although deformations are much less pronounced than in our DFT study. This holds especially for the remarkable shift of the abstracted proton from C^β to C^α, which we have found to occur in the anti-E2 reaction of F^- and C_2H_5F. In the HF/3-21G(+p) structure for the TS(anti-E2), the β-proton has been displaced only very slightly in the same direction ($\angle HC^\beta C^\alpha$ decreases from 110° in st-C_2H_5F via 106° in RC(st) to 99° in TS(anti-E2)).[55] The same trend has also been observed for the anti-E2 reactions of F^- and Cl^- with C_2H_5Cl.[56] Apparent differences between our results and those of Minato and Yamabe[56] are their considerably higher activation barriers and the reversed energetic order of the anti-E2 and S_N2 transition states, respectively, which have been calculated to be above the separated reactants F^- and staggered fluoroethane by 0.65 and 0.43 eV at the RHF/DZP//RHF/3-21G(+p) level and by 0.36 and 0.05 eV at the MP3/3-21G(+p)//RHF/3-21G(+p) level of theory. Furthermore, the RHF/3-21G(+p) imaginary frequencies associated with the transition states (TS(anti-E2), *i* 326 cm^{-1}; TS(S_N2), *i* 572 cm^{-1})[55,56] are significantly higher than those obtained in this work at the Xα level of DFT (TS(anti-E2), *i* 98 cm^{-1}; TS(S_N2), *i* 387 cm^{-1}; Figure 2c). These differences may be ascribed partly to the much smaller basis set used in the *ab initio* study. However, it is well-known that *ab initio* theory fails to describe processes of bond breaking adequately at the HF level ("improper dissociation"). As a result, activation barriers and vibrational frequencies may be overestimated considerably. This deficiency can be reduced by the incorporation of correlation, but sometimes very high levels of *ab initio* theory (up to MC10/DZP) are required to approach an appropriate accuracy.[85] In contrast, some evidence has been obtained now[85] that local DF methods, although providing satisfactory vibrational frequencies, underestimate activation barriers, whereas at the LDA/NL level activation barriers are obtained which are in excellent agreement with experiment. It therefore appears that DF and conventional *ab initio* results converge with increasing level of theory, one from above, the other one from below[85] (exactly this effect has been noted for the proton transfer in $CH_4\cdots CH_3^-$ in ref 73).

A quantitative comparison between our results and those obtained by Gronert[60,61] at various levels of conventional *ab initio* theory is less straightforward because these studies do not have an investigated reaction system in common. However, the preference of anti-E2 over syn-E2 elimination which was found for the reaction of $F^- + C_2H_5Cl$[61] parallels our results for the reaction of $F^- + C_2H_5F$.

An interesting comparison can be made between our results and those obtained from AM1 calculations of Dewar and Yuan[63] on the gas-phase reactions between methoxide and chloroalkanes ($B^- = CH_3O^-$ and L = Cl in eq 1) and between ammonia and alkylhydroxonium cations ($B^- = NH_3$ and $L = OH_2^+$ in eq 1). From this study,[63] it follows that the E2 reaction prevails in the anionic reaction system involving chloroethane, while the S_N2 reaction dominates in the cationic reaction system involving alkylhydroxonium. This is in full agreement with expectations based on our qualitative analysis of the nature of the substrate LUMO (Scheme III). The anionic reaction system closely resembles our model system $F^- + C_2H_5F$ and corresponds to a situation where the substrate LUMO has much C^β–H σ^* antibonding character; thus the reaction system is predestined to undergo E2 elimination (Scheme III, left). On the other hand, the σ^* and π^* levels of the CH_2L^+ fragment in the alkylhydroxonium cation are considerably stablized due to the field effect of the positive charge. Consequently, the substrate LUMO is expected to have considerable C^α–L σ^* antibonding character; the S_N2 substitution is therefore expected to be considerably enhanced with respect to the E2 elimination (Scheme III, right). In fact, these results are confirmed by gas-phase experiments:[19-33,89] whereas, in general, E2 reactions dominate in gas-phase anion/molecule reactions,[19-33] the S_N2 reaction prevails in the reaction between ammonia and the diethylmethyloxonium cation ($B^- = NH_3$ and $L = O(CH_3)(C_2H_5)^+$ in eq 1).[89]

Recent gas-phase (FA) studies[90] on anion/molecule reactions involving ethyl dimethyl phosphate as the neutral substrate have shown that the intrinsic competition between E2 and S_N2 mechanisms is, most importantly, controlled by the nucleophilic structure. Bases containing a hard localized nucleophilic center, e.g. F, N, or O, react preferentially via the E2 pathway, whereas bases with a soft diffuse nucleophilic center, e.g. C or S, prefer to react via the S_N2 channel.[90] This observation nicely confirms our expectations with respect to the influence of the electronic structure of the base on the E2 *versus* S_N2 selectivity (*vide supra*).

Our results are in excellent agreement with experimental results of low-pressure gas-phase (ICR) studies by Ridge and Beauchamp.[22,23] In the reaction of F^- with fluoroethane, the exclusive formation of FHF^- is observed, which has to proceed via elimination (eq 3). This fits in nicely with the strong prevalence

$$F^- + C_2H_5F \longrightarrow FHF^- + C_2H_4 \qquad (3)$$

of E2 over S_N2 inferred from our calculations. However, the FHF^- complex is not ncessarily formed via syn elimination as suggested by Ridge and Beauchamp.[22,23] From our calculations, it follows that the anti-E2 reaction also preferentially leads to the 1.75 eV exothermic FHF^- production and is strongly favored over the syn-E2 reaction (Figure 3b). The absence of F^- ions from anti-E2 is easily explained as this reaction channel is endothermic by 0.29 eV and, thus, is not available under low-pressure conditions.[32,33] The nonappearance of [C_2H_4, F^-] is ascribed to the much less favorable reaction energy of the channel leading to products P2 (–0.02 eV, Table I) and is consistent with

(89) Occhiucci, G.; Speranza, M.; de Koning, L. J.; Nibbering, N. M. M. *J. Am. Chem. Soc.* **1989**, *111*, 7387.
(90) Lum, R. C.; Grabowski, J. J. *J. Am. Chem. Soc.* **1992**, *114*, 9663.

a preferential collapse of the TS(anti-E2) toward PC1 or PC2 (Figures 3b and 4a).

Expectations for the Condensed Phase. Finally, the relevance of our gas-phase results for condensed-phase reactions is qualitatively evaluated. In the condensed phase, the reactants are stabilized by solvation. This stabilization is, probably, most pronounced for the separated reactants and products because the rather compact F^- and FHF^- anions can have a very favorable electrostatic and/or charge-transfer (hydrogen bond) interaction with solvent molecules. Both the E2 and S_N2 reactions can only proceed via partial desolvation of reactants in order to form the reactant complex. The change in the mutual competition between E2 and S_N2 upon solvation is difficult to trace. Inspection of the charge distribution of the transition states in Figure 8 shows that the TS(S_N2) contains two relatively "naked" fluorine atoms and may benefit the most by solvation. This would be in agreement with the relative ease of condensed-phase S_N2 reactions,[1,2] if compared with the strong prevalence of E2 reactions in the gas phase.[32,33] Nevertheless, this is speculative and more detailed investigations are under way to tackle this problem.

5. Conclusion

In this paper we have investigated the nature of the base-induced elimination reaction using F^- and fluoroethane as a model reaction system. The base has been found to play a key role as a catalyst which also strongly influences the competition between anti and syn elimination. The thermal elimination of HF from fluoroethane preferentially proceeds via the syn pathway. Upon catalysis by the base, the transition states are considerably stabilized. This stabilization, however, selectively favors the anti mode, leading to the prevalence of anti-E2 over syn-E2 elimination. One reason for the selective stabilization is the very low energy and, thus, the good acceptor capability of the C_2H_5F 8a′ LUMO (σ antibonding for CC–H and C^α–F, Figure 6b) in the strongly rearranging, loose anti-E2 transition state. The second factor is the stabilizing electrostatic interaction of the F^- base with the fluoroethane substrate, mostly because of the favorable magnitude and orientation of the C^α–F dipole moment in the anti-E2 TS structure. One way to view this result is that a loose TS structure, with a long C^α–F bond and strongly negative leaving F (see Figure 8), is favored in the anti-E2 for electrostatic reasons; the necessarily high distortion energy of the substrate is not prohibitive since the concomitant lowering of the 8a′ energy leads to strong donor/acceptor interaction with the F^- base. The important role for interaction with the attacking base does not seem to support the traditional view that stabilization of the anti-E2 TS is caused by favorable interaction of a developing carbanionic lone pair at C^β with the backside lobe of the $\sigma^*(C^\alpha–F)$.

There are several reasons for the preference of the gas-phase base-induced elimination over the nucleophilic substitution. The base F^- preferentially combines with the C_2H_5F substrate to form a reactant complex that is predestined to undergo anti-E2 elimination. Furthermore, the activation barrier for elimination is considerably lower (for anti-E2) and the transition states are more loosely bound and thus correspond to a situation with a relatively high density of states, i.e. a less negative and thus favorable activation entropy.

A qualitative MO theoretical analysis has been presented, which enables one to understand and predict which reaction, E2 or S_N2, dominates for a given general substrate C_2H_5L. The E2 reaction is favored in the case that the $CH_2L^\bullet$ π^* orbital is higher in energy than the $CH_3^\bullet$ σ^* due to the strong C^β–H σ^* antibonding character of the substrate LUMO (Scheme III, left hand side). When the energy of the $CH_2L^\bullet$ π^* orbital falls below that of $CH_3^\bullet$ σ^*, the LUMO becomes essentially C^α–L σ^* antibonding and, therefore, the S_N2 reaction becomes competitive (Scheme III, right hand side). In intermediate situations, the substrate LUMO will have comparable amounts of C^β–H σ^* and C^α–L σ^* antibonding character. This opens the possibility of an E2C-like mechanism (Figure 1). In this way, the VTS model for E2 eliminations is coupled to that for S_N2 substitutions by a simple MO theoretical concept which depends on the relative height of the $CH_3^\bullet$ σ^* and the $CH_2L^\bullet$ π^* orbitals. The resulting "E2/S_N2 spectrum" thus covers a range of reaction mechanisms which extends from E2H via E2C to S_N2, i.e. it comprises the Bunnet–Cram, the Winstein–Parker, and the S_N2/S_N1 spectra.[1,2] It is emphasized that for a given substrate the electronic structure of the base should determine the E2 *versus* S_N2 selectivity. Hard localized bases are expected to react preferentially via the E2 pathway, whereas soft diffuse bases are expected to prefer the S_N2 channel, on the basis of qualitative overlap considerations.

The base-induced syn-E2 elimination of F^- and C_2H_5F is E1cb-like. Nevertheless, the inversion of configuration proposed in the "internal S_N2" concept does not occur. The geometry of the anti-E2 transition state is virtually central E2. However, on the reaction energy surface (Figure 4a), there is no direct channel toward the transition state involving synchronous C^β–H and C^α–F bond breaking. Instead, there is a very weak preference for an asynchronous pathway (either E1cb-like or E1-like). Furthermore it is concluded that the anti-E2 reaction is of the E2H type (Figure 1), as no E2C-like interactions are present in the transition state. Finally, an important characteristic of the anti-E2 elimination is the pronounced shift of the abstracted proton from the C^β to the C^α position in the transition state. This feature is not contained in the E2H formalism.

Acknowledgment. The authors thank the Netherlands Organization for Scientific Research (NCF/NWO) for financial support.